Prepared for submission to JHEP DESY-25-167

Extracting Mellin moments of double parton distributions from lattice data

Markus Diehl,[a] **Oskar Grocholski,**[a,b] **Daniel Reitinger,**[c] **Andreas Schäfer**[c,d] **and Christian Zimmermann**[e,f]

[a] *Deutsches Elektronen-Synchrotron DESY, Notkestr 85, 22607 Hamburg, Germany*
[b] *Irfu, CEA, Université Paris-Saclay, F-91191, Gif-sur-Yvette, France*
[c] *Institute for Theoretical Physics, University of Regensburg, 93040 Regensburg, Germany*
[d] *Department of Physics, National Taiwan University, Taipei 106, Taiwan*
[e] *Department of Physics and Astronomy, University of Kentucky, Lexington, KY 40506, USA*
[f] *Nuclear Science Division, Lawrence Berkeley National Laboratory, Berkeley, CA 94720, USA*

E-mail: Daniel.Reitinger@physik.uni-regensburg.de

Abstract: Reconstructing Mellin moments of double parton distributions from calculations on a Euclidean lattice requires taking an integral over a variable that may be regarded as a Ioffe time. The Fourier conjugate of this variable plays the role of a kinematic skewness in the double parton distributions. We discuss the skewness dependence of the relevant hadronic correlation functions. Using several models, we study the impact of this dependence on extracting moments of double parton distributions from existing lattice data.

ArXiv ePrint: 2511.15546

Contents

1 Introduction

The LHC is presently the leading accelerator searching for New Physics at the energy frontier and will stay so for many years to come. To make best use of its data, significant theory efforts are required, in particular in the domain of strong interaction physics. Among the open challenges in this area is a better understanding of multiparton interactions, which for particular final states could mimic or hide signals for New Physics. In multiparton interactions, several hard processes occur in the same proton-proton collision. The simplest and most prominent case is double parton scattering, in which two partons from each proton take part in a hard scattering. A comprehensive overview of this subject can be found in [1].

The initial state of double parton scattering is described by double parton distributions (DPDs). Whereas single parton distributions (PDFs) have entered the realm of precision physics, our knowledge of DPDs remains quite fragmentary. This has several reasons, ranging from their inherent complexity (they depend on two parton labels, three variables, two scales) to the difficulties of extracting double parton scattering from experimental measurements. In this situation, theoretical input that allows us to constrain these functions is of great value. Beyond their practical relevance for collider physics, DPDs are of interest in themselves, because they describe quantum correlations inside the proton that are "invisible" in single-parton distributions.

It is natural to ask how lattice QCD can inform us about DPDs, given the long and successful history of studying single-parton distributions on the lattice (see [2, 3] for recent reviews). In this context, one may distinguish two different approaches.

1. Mellin moments of PDFs are related to hadronic matrix elements of local currents, which are well suited for evaluation on a Euclidean lattice. This method has reached a high degree of sophistication regarding the reliability of results (see Section II in [3]), but due to power-divergent operator mixing most studies so far are limited to the lowest three moments. While three moments are not sufficient to reconstruct the dependence of PDFs on their momentum fraction x, they may for instance be used as additional input in PDF fits to experimental data. Moreover, some of the moments are related to sum rules and of interest in themselves, such as the lowest moments of helicity dependent PDFs.

   As pointed out in [4], this method can be extended to DPDs by relating their Mellin moments to the hadronic matrix elements of two currents at different spatial positions. Computationally this is much more demanding since it requires the evaluation of four-point functions on the lattice (instead of three-point functions for PDFs). Nevertheless, we have shown in a series of studies [5–7] that good statistical signals can be obtained for a variety of correlation functions related to the lowest Mellin moments of DPDs in the pion or the nucleon.

   There is, however, a further complication: to reconstruct the Mellin moments of DPDs with this method, one needs to evaluate the integral over a variable ω that may be regarded as a Ioffe time and physically ranges from $-\infty$ to $+\infty$. In lattice simulations one can only access a finite range in this variable. In our previous work, we tackled this problem by introducing a kinematical "skewness" variable ζ that is Fourier conjugate to ω, such that the Mellin moments of DPDs correspond to $\zeta = 0$. We then assumed a simple functional form for this ζ dependence and determined its parameters by fits to the lattice data.

   The purpose of the present work is to take a closer look at this procedure, exploring a broader range of physically motivated ansätze for the ζ dependence and investigating the corresponding fit results.

2. A variety of methods have been proposed for accessing the x dependence of PDFs in a more direct manner, see e.g. section 2 in [2]. In particular, the concepts of quasi-

distributions [8, 9] and of pseudo-distributions [10, 11] have been employed in recent years to probe the x dependence of single-parton quantities, not only for PDFs but also for TMDs (transverse momentum distributions) and GPDs (generalized parton distributions).

Incidentally, the problem described above — having to integrate over Ioffe time for obtaining the quantities of physical interest — also occurs for quasi- and pseudo-distributions, where, roughly speaking, a Ioffe time variable is Fourier conjugate to the momentum fraction x. Also in these cases, lattice simulations are restricted to a finite range in this variable. This issue is under active investigation, see for instance [12], [13], [14], and references therein.

An extension of the quasi-distribution method to DPDs has been formulated in [15] and [16]. The impressive progress achieved with this method for single-parton distributions raises hope that it can be turned into a powerful tool to learn more about DPDs as well. We shall, however, not pursue this avenue in the present work.

This work is organized as follows. In Section 2 we recall the most important properties of DPDs, their extension to finite skewness ζ, as well as their relation with hadronic matrix elements of two local currents. In Section 3 we derive constraints on the ζ dependence of Mellin moments of DPDs. The most important aspects of our lattice analysis are recalled in Section 4. We introduce different parameterizations for the ζ-dependent moments in Section 5 and use these to fit the lattice data in Section 6. We summarize our findings in Section 7.

2 Theory background

In this section, we review basic definitions and properties of DPDs, including their extension to nonzero skewness ζ introduced in our previous lattice studies [5, 6].

2.1 DPDs, skewed DPDs, and their Mellin moments

DPDs are defined by matrix elements of the product of two twist-two operators. Throughout this work, we consider only twist-two operators in the color singlet representation, i.e. without open color indices. For simplicity, we also restrict ourselves to the case of unpolarized partons, where our lattice data is most precise. An extension of our theoretical arguments to polarized partons is straightforward.

We use light cone coordinates $v^{\pm} = \left(v^0 \pm v^3\right)/\sqrt{2}$ and $\boldsymbol{v} = \left(v^1, v^2\right)$ for a given four-vector v^μ. The twist-two operators for an unpolarized quark or antiquark read

$$\begin{aligned}
\mathcal{O}_q(y,z) &= \frac{1}{2}\,\bar{q}\left(y - \frac{1}{2}z\right)\gamma^+\,q\left(y + \frac{1}{2}z\right)\Big|_{z^+=y^+=0,\,\boldsymbol{z}=\boldsymbol{0}}\,, \\
\mathcal{O}_{\bar{q}}(y,z) &= -\frac{1}{2}\,\bar{q}\left(y + \frac{1}{2}z\right)\gamma^+\,q\left(y - \frac{1}{2}z\right)\Big|_{z^+=y^+=0,\,\boldsymbol{z}=\boldsymbol{0}}\,,
\end{aligned} \tag{2.1}$$

respectively, where we have suppressed the usual Wilson line along the straight path from $y - \frac{1}{2}z$ to $y + \frac{1}{2}z$. The operator $\mathcal{O}_g$ for gluons can for instance be found in Section 2.2

of [4]. It is understood that ultraviolet divergences are renormalized in the conventional way, using the $\overline{\text{MS}}$ prescription. The corresponding scale dependence of operators and their matrix elements is suppressed for brevity in all of this work. The DPD for unpolarized partons a_1 and a_2 is then defined by

$$F_{a_1a_2}\left(x_1, x_2, y^2\right) = 2p^+ \int \mathrm{d}y^- \int \frac{\mathrm{d}z_1^-}{2\pi} \frac{\mathrm{d}z_2^-}{2\pi} e^{i\left(x_1 z_1^- + x_2 z_2^-\right)p^+} \times {\sum_\lambda}' \left\langle p, \lambda \right| \mathcal{O}_{a_1}(y, z_1)\, \mathcal{O}_{a_2}(0, z_2) \left| p, \lambda \right\rangle \,. \tag{2.2}$$

Here we have taken the average over the proton polarization λ, which we write as ${\sum_\lambda}' = \frac{1}{2}\sum_\lambda$. We work in a frame where the transverse momentum $\boldsymbol{p}$ of the proton is zero. Due to rotational invariance, the DPD then depends on the transverse distance $\boldsymbol{y}$ between the two partons only via the Lorentz invariant

$$y^2 = -\boldsymbol{y}^2 \,. \tag{2.3}$$

The matrix element in (2.2) has support for both positive and negative plus-momentum fractions x_i $(i = 1, 2)$, where $x_i > 0$ corresponds to extracting a parton a_i and $x_i < 0$ corresponds to extracting the charge conjugate parton $\bar{a}_i$.[1]

The extension of this definition to nonzero skewness ζ reads

$$F_{a_1a_2}\left(x_1, x_2, \zeta, y^2\right) = 2p^+ \int \mathrm{d}y^- e^{-i\zeta y^- p^+} \int \frac{\mathrm{d}z_1^-}{2\pi} \frac{\mathrm{d}z_2^-}{2\pi} e^{i\left(x_1 z_1^- + x_2 z_2^-\right)p^+} \times {\sum_\lambda}' \left\langle p, \lambda \right| \mathcal{O}_{a_1}(y, z_1)\, \mathcal{O}_{a_2}(0, z_2) \left| p, \lambda \right\rangle \,. \tag{2.4}$$

Compared with (2.2), we now have an additional phase factor that involves the Lorenz invariant

$$\omega = py = p^+ y^- \,, \tag{2.5}$$

which we refer to as a Ioffe time. This variable is Fourier conjugate to the skewness ζ. Due to parity and time reversal invariance, one has the symmetry property

$$F_{a_1a_2}\left(x_1, x_2, \zeta, y^2\right) = F_{a_1a_2}\left(x_1, x_2, -\zeta, y^2\right) \,. \tag{2.6}$$

The skewness parameter introduces a difference between the momentum fractions of the partons in the bra or ket states of the matrix element, viz. in the wave function or the conjugate wave function of the proton. Positive momentum fractions $x_1 - \zeta/2$ $(x_2 + \zeta/2)$ correspond to a parton a_1 (a_2) in the wave function, and positive momentum fractions $x_1 + \zeta/2$ $(x_2 - \zeta/2)$ to a parton a_1 (a_2) in the conjugate wave function, as shown in Figure 1a. When $x_1 - \zeta/2$ turns from positive to negative values, a_1 in the wave function turns into $\bar{a}_1$ in the conjugate wave function, with corresponding statements for the other three momentum

[1] For brevity, we use the term "momentum fraction" instead of "plus-momentum fraction" from now on.

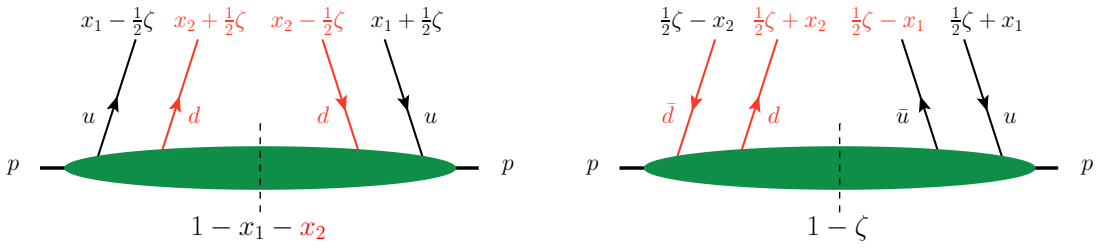

(a) $x_i \pm \zeta/2 > 0$ (b) $\zeta/2 \pm x_i > 0$

Figure 1. Illustration of the skewed DPD $F_{ud}\left(x_1, x_2, \zeta, y^2\right)$ for the cases where (a) all fractions $x_i \pm \zeta/2$ or (b) all fractions $\zeta/2 \pm x_i$ are positive. Below the vertical dashed line we give the total momentum fraction carried by the spectator partons.

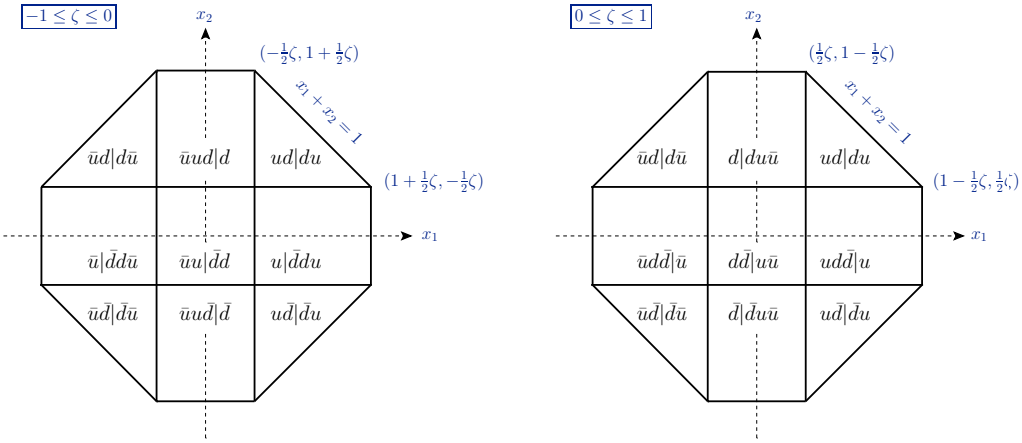

Figure 2. Support regions of $F_{ud}\left(x_1, x_2, \zeta, y^2\right)$ in the (x_1, x_2)-plane for negative (left) and positive (right) values of ζ. For each region we indicate the (anti-)quark content of the wave function and its complex conjugate. The notation $u|\bar{d}du$ means that we have a u-quark in the proton wave function and $\bar{d}du$ in its complex conjugate.

fractions. Figure 1b shows the configuration with $a_2\bar{a}_2$ in the wave function and $a_1\bar{a}_1$ in the conjugate wave function.

Using the methods of [17], one can show that the support property of the matrix element in (2.4) is [5]

$$\left|x_i \pm \frac{1}{2}\zeta\right| \le 1\,, \quad |x_1| + |x_2| \le 1\,, \quad |\zeta| \le 1\,. \tag{2.7}$$

The different parts of the support region and their partonic interpretation are visualized in Figure 2.

When taking Mellin moments in the momentum fractions x_1 and x_2, the non-local twist-two operators in (2.2) and (2.4) turn into local currents. For the lowest Mellin moment we

have

$$I_{a_1a_2}(\zeta, y^2) = \int_{-1}^{1} \mathrm{d}x_1 \int_{-1}^{1} \mathrm{d}x_2 \, F_{a_1a_2}(x_1, x_2, \zeta, y^2)$$
$$= \frac{2}{(p^+)^2} \int \mathrm{d}\omega \, e^{-i\zeta\omega} \sum_{\lambda}{}' \, \langle p, \lambda | \, \mathcal{O}_{a_1}(y, 0) \, \mathcal{O}_{a_2}(0, 0) \, | p, \lambda \rangle \,, \tag{2.8}$$

where it is understood that the integrals over x_1 and x_2 are performed over the full support region shown in Figure 2. The symmetry property (2.6) for skewed DPDs implies

$$I_{a_1a_2}(\zeta, y^2) = I_{a_1a_2}(-\zeta, y^2) \,. \tag{2.9}$$

2.2 The number sum rule

DPDs fulfill sum rules, which have been proposed in [18] and proven in [19, 20]. In the context of our lattice calculations, only the number sum rule is relevant. For the two-quark DPD $F_{qq'}$ it can be written as

$$2\pi \int_{y_{\text{cut}}}^{\infty} \mathrm{d}y \, y \int_{-1+|x_1|}^{1-|x_1|} \mathrm{d}x_2 \, F_{qq'}(x_1, x_2, y^2)$$
$$= \begin{cases} \big(N_{q'} - \delta_{qq'}\big) \, f_q(x_1) + \mathcal{O}\big(\alpha_s\big) + \mathcal{O}(\Lambda^2 y_{\text{cut}}^2) & \text{for } x_1 > 0 \,, \\ -\big(N_{q'} + \delta_{qq'}\big) \, f_{\bar{q}}(-x_1) + \mathcal{O}\big(\alpha_s\big) + \mathcal{O}(\Lambda^2 y_{\text{cut}}^2) & \text{for } x_1 < 0 \,, \end{cases} \tag{2.10}$$

where f_q and $f_{\bar{q}}$ are the usual quark and antiquark distributions and $N_{q'}$ is the number of valence quarks q'. To obtain this form, we have used the relation $F_{\bar{q}q'}(x_1, x_2, y^2) = -F_{qq'}(-x_1, x_2, y^2)$ and its counterpart for the second parton, which follow from the relation between quark and antiquark operators in (2.1).

As discussed in [20], the lower cutoff on the integral over y is necessary to deal with the singular $1/y^2$ behavior of $F_{qq'}$ at $y \to 0$. This behavior is due to perturbative splitting and comes with at least one factor of α_s. The last term in (2.10) denotes power corrections, with Λ representing a typical hadronic scale. One should therefore take y_{cut} sufficiently small. We use $y_{\text{cut}} = b_0/\mu$, where μ is the renormalization scale of the DPD and $b_0 = 2e^{-\gamma} \approx 1.12$ with the Euler-Mascheroni constant γ. Taking $\mu = 2\,\text{GeV}$ we get

$$y_{\text{cut}} \approx 0.11\,\text{fm} \,. \tag{2.11}$$

In Section 5.2 we comment on the dependence of the integral over y on its boundaries.

When considering Mellin moments in both momentum fractions, we want to integrate (2.10) over x_1. This is only well defined for $q \neq q'$, because the corresponding expression for $q = q'$ includes sea quark contributions that lead to divergent results when integrated over all momentum fractions. Taking the parton combination ud in (2.10) and using the number sum rule for ordinary PDFs, we get

$$S_{ud}(y_{\text{cut}}) = 2\pi \int_{y_{\text{cut}}}^{\infty} \mathrm{d}y \, y \, I_{ud}(\zeta = 0, y^2) = 2\pi \int_{y_{\text{cut}}}^{\infty} \mathrm{d}y \, y \int_{-1}^{1} \mathrm{d}x_1 \int_{-1}^{1} \mathrm{d}x_2 \, F_{ud}(x_1, x_2, y^2)$$
$$= 2 + \mathcal{O}(\alpha_s^2) + \mathcal{O}(\Lambda^2 y_{\text{cut}}^2) \,. \tag{2.12}$$

Notice that the power of α_s on the r.h.s. is higher than in the generic relation (2.10), because perturbative splitting for the parton combination ud starts only at order α_s^2.

2.3 Two-current matrix elements

The relation between two-current matrix elements and DPDs has been worked out in detail in [5, 6]. For the present work, we need the correlation function

$$M^{\mu_1\mu_2}_{q_1q_2,VV}(p,y) = \sum_\lambda{}' \, \langle p,\lambda | \, J^{\mu_1}_{q_1,V}(y) \, J^{\mu_2}_{q_2,V}(0) \, | p,\lambda \rangle \tag{2.13}$$

of two quark vector currents

$$J^\mu_{q,V}(y) = \bar{q}(y) \gamma^\mu q(y) \,. \tag{2.14}$$

This matrix element can be decomposed in terms of Lorentz invariant functions, which depend on the Lorentz scalars $\omega = py$ and y^2 only. Symmetrizing the tensor (2.13) and subtracting its trace, we get

$$\begin{aligned} &\tfrac{1}{2}\big(M^{\mu\nu}_{q_1q_2,VV} + M^{\nu\mu}_{q_1q_2,VV}\big) - \tfrac{1}{4} g^{\mu\nu} g_{\alpha\beta} M^{\alpha\beta}_{q_1q_2,VV} \\ &\quad = u^{\mu\nu}_{VV,A} \, A_{q_1q_2}(\omega,y^2) + u^{\mu\nu}_{VV,B} \, m^2 \, B_{q_1q_2}(\omega,y^2) + u^{\mu\nu}_{VV,C} \, m^4 \, C_{q_1q_2}(\omega,y^2) \end{aligned} \tag{2.15}$$

with tensors $u^{\mu\nu}$ given in Section 2.3 of [6]. Comparing this with the matrix element representation (2.8) of the Mellin moment $I_{q_1q_2}$, one finds

$$I_{q_1q_2}(\zeta,y^2) = \int_{-\infty}^{\infty} \mathrm{d}\omega \, e^{-i\zeta\omega} \, A_{q_1q_2}(\omega,y^2) \,, \tag{2.16}$$

$$A_{q_1q_2}(\omega,y^2) = \frac{1}{2\pi} \int_{-1}^{1} \mathrm{d}\zeta \, e^{i\zeta\omega} \, I_{q_1q_2}(\zeta,y^2) \,, \tag{2.17}$$

where in the second line we have used the limited support of $I_{q_1q_2}$ in ζ. These relations imply that $A_{q_1q_2}(\omega,y^2)$ is even in ω, because $I_{q_1q_2}(\zeta,y^2)$ is even in ζ.

The distance y between the twist-two operators in DPDs is always spacelike, as can be seen in (2.3). One also gets spacelike y if one sets $y^0 = 0$ in the two-current correlators (2.13), which can then be evaluated in Euclidean space-time. From this one can extract the invariant functions $A_{q_1q_2}(\omega,y^2)$, which appear in (2.16). We thus have the situation announced in the introduction. Our primary physics interest is in the Mellin moments $I_{q_1q_2}(\zeta = 0,y^2)$ of DPDs at zero skewness, since these DPDs appear in double parton scattering. To evaluate the Mellin moments from correlation functions accessible to lattice simulations, we need to perform an integral over the Ioffe time ω.

3 Properties of Mellin moments

Little is known about the functional form of the Mellin moments $I_{a_1a_2}(\zeta,y^2)$, apart from the symmetry constraint that they are even functions of ζ. In our previous analysis [6] of lattice results, we assumed a polynomial form in ζ. Whilst this ansatz produced stable fits to the data for $A_{a_1a_2}(\omega,y^2)$, we now show that it misses an important boundary condition and at the same is too restrictive. Specifically, we argue that

1. $I_{a_1a_2}(\zeta,y^2)$ should vanish rather fast in the limit $\zeta \to 1$,

2. in general, $I_{a_1a_2}(\zeta, y^2)$ is not an analytic function of ζ at the points $\zeta = 0$ and $\zeta = 1$.

Throughout this section will assume $\zeta \geq 0$ for ease of notation, bearing in mind that $I_{a_1a_2}(\zeta, y^2)$ is even in ζ.

The first property follows from a rather general physics consideration. As $\zeta \to 1$, the support of skewed DPDs in x_1 and x_2 reduces to the central square $|x_1|, |x_2| \leq \frac{1}{2}\zeta$ in Figure 2. The corresponding parton configuration is the one shown in Figure 1b, where the two extracted partons together carry a longitudinal fraction ζ of the proton momentum, leaving a fraction $1 - \zeta$ for the remaining spectator partons. More specifically, for the parton combinations $(a_1a_2) = (ud), (uu), (dd)$ accessible in our lattice data, the moment $I_{a_1a_2}$ at $\zeta = 1$ describes the extraction of a color-singlet $u\bar{u}$ or $d\bar{d}$ pair that carries the full longitudinal proton momentum, with zero longitudinal momentum of the remaining partons (which include two or three "valence quarks" if one regards the proton as a system made from three valence quarks plus sea quarks and gluons). We find it plausible that the probability for such configurations is zero and that the approach to zero should be fast as $\zeta \to 1$, to a similar extent as ordinary u or d quark PDFs quickly approach zero as their momentum fraction x tends to 1.

Somewhat unfortunately, the region $\zeta \approx 1$ constrained by this argument is far away from the limit $\zeta \to 0$ that brings us to ordinary (non-skewed) DPDs and the physics of double parton scattering. In the following subsection we therefore present an argument for the second property stated above.

3.1 Lessons from the small-distance limit

As shown in [4, 21], ordinary DPDs in the limit of small interparton distance y are dominated by the mechanism in which the two extracted partons originate from the splitting of a single parton. One can then compute the DPD in terms of ordinary PDFs and perturbative splitting kernels. The arguments for this type of factorization extend to the case of nonzero skewness ζ. Corresponding Feynman graphs are shown in Figure 3.

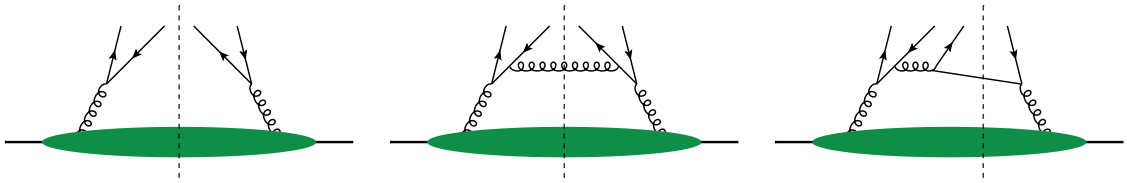

Figure 3. Graphs for the perturbative splitting mechanism of DPDs at leading (a) or next-to-leading (b, c) order in α_s. Graph (c) only contributes for $\zeta \neq 0$.

At leading order (LO) in α_s, the graph in Figure 3a can contribute to DPDs in the regions given by the triangles $|x_1| \geq \frac{1}{2}\zeta$, $|x_2| \geq \frac{1}{2}\zeta$ in the (x_1, x_2) plane. Since the quark-antiquark pairs on either side of the final-state cut are coupled to a color octet in this graph, it does not populate the central square $|x_1| \leq \frac{1}{2}\zeta$, $|x_2| \leq \frac{1}{2}\zeta$, which corresponds to extracted quark-antiquark pairs in a color singlet. By contrast, the next-to-leading order

(NLO) graph in Figure 3b contributes to both the triangles and the central square in the support octagon. NLO graphs such as the one in 3c populate the outer rectangles where $|x_1| \geq \frac{1}{2}\zeta$ and $|x_2| \leq \frac{1}{2}\zeta$ or vice versa.

We will shortly discuss the contribution of the LO graph for $g \to q\bar{q}$ splitting to the Mellin moment I_{qq}. Before doing so, we should point out that this contribution has no direct connection to the lattice data analyzed in this work. For one thing, distances y small enough for a perturbative treatment correspond to less than one or two units of the lattice spacing $a \approx 0.0856\,\text{fm}$, and at such distances we must expect significant discretization effects. Moreover, the perturbative graphs in Figure 3 correspond to the lattice contraction S_2 in Figure 4, which will be excluded from our numerical analysis for the reasons given in Section 4.2 . However, for showing that it is *not a general property* of the Mellin moments $I_{a_1 a_2}(\zeta, y^2)$ to be analytic functions of ζ at $\zeta = 0$ or $\zeta = 1$ it is sufficient to consider a restricted region of y, a restricted set of contributing graphs or lattice contractions, and a particular combination of the partons a_1 and a_2.

As shown in appendix A, the contribution of Figure 3a to the lowest Mellin moment of F_{qq} reads

$$I_{qq}(\zeta, y^2) = -\frac{2}{\pi |y^2|} \frac{\alpha_s}{2\pi} T_F \int_\zeta^1 \mathrm{d}z \, f_g(z) \, \frac{1}{3} \left(1 - \frac{\zeta}{z}\right)^2 \left(2 + \frac{\zeta}{z}\right). \tag{3.1}$$

where $T_F = 1/2$ and $f_g(z)$ is the gluon distribution in the proton. Assuming a behavior

$$f_g(z) \sim z^{-1+\alpha} \, (1-z)^\beta \qquad \text{with } -1 < \alpha < 0 \tag{3.2}$$

and β much larger than unity, one finds that

$$I_{qq}(\zeta, y^2) \sim \int_\zeta^1 \mathrm{d}z \, (1-z)^\beta \, (z-\zeta)^2 \sim (1-\zeta)^{3+\beta} \qquad \text{for } \zeta \to 1\,. \tag{3.3}$$

This provides a concrete example for our expectation that the Mellin moment vanishes rather fast as $\zeta \to 1$.

With the condition on α in (3.2), the integral in (3.1) diverges as $\zeta \to 0$, and one finds a singular behavior

$$I_{qq}(\zeta, y^2) \sim \zeta^\alpha \qquad \text{for } \zeta \to 0\,. \tag{3.4}$$

This is closely related to fact the lowest Mellin moment $\int_0^1 \mathrm{d}z \, f_g(z)$ of the gluon PDF is divergent as well. It is also in line with the observation we made in Section 2.2, namely that the DPD number sum rule for equal quark flavors gives infinity when integrated over *both* momentum fractions.

It is instructive to consider in addition the Mellin moment with weight factor $x_1 x_2$, for which the leading order perturbative splitting gives

$$\begin{aligned} I_{qq}^{(2,2)}(\zeta, y^2) &= \int_{-1}^1 \mathrm{d}x_1 \, x_1 \int_{-1}^1 \mathrm{d}x_2 \, x_2 \, F_{qq}(x_1, x_2, \zeta, y^2) \\ &= \frac{2}{\pi |y^2|} \frac{\alpha_s}{2\pi} T_F \int_\zeta^1 \mathrm{d}z \, z^2 \, f_g(z) \, \frac{1}{60} \left(1 - \frac{\zeta}{z}\right)^2 \left(6 + \frac{12\zeta}{z} - \frac{2\zeta^2}{z^2} - \frac{\zeta^3}{z^3}\right). \end{aligned} \tag{3.5}$$

One easily finds that for a gluon distribution of the form (3.2) this has same behavior at $\zeta \to 1$ as $I_{qq}(\zeta, y^2)$ in (3.3). Thanks to the factor z^2 in the integrand, it has a finite value at $\zeta = 0$, but it is non-analytic at that point.

In summary, the above example shows that a non-analytic behavior of PDFs at momentum fraction $z = 0$ and $z = 1$ induces a non-analytic behavior of Mellin moments of DPDs at skewness $\zeta = 0$ and $\zeta = 1$ if the distance y is sufficiently small. It is difficult to imagine how the same Mellin moments could be analytic in ζ at larger values of y, where the perturbative splitting formula for DPDs does not hold.

4 Lattice calculation

In this section we recall the basic steps for extracting the invariant functions $A_{q_1 q_2}(\omega, y^2)$ from lattice simulations. For details and plots we refer to the reader to our previous work [6].

4.1 Two-current matrix elements

In order to evaluate the two-current matrix element (2.13) on the lattice, we switch from Minkowski space to Euclidean space. As is customary, the corresponding time component is labeled by the index 4 instead of 0. We then define the following four-point function for the proton:

$$C^{VV,\vec{p}}_{4\text{pt},qq'}(\vec{y}, t, \tau) = a^6 \sum_{\vec{z}',\vec{z}} e^{-i\vec{p}(\vec{z}'-\vec{z})} \left\langle \text{tr}\left\{ P_+ \mathcal{P}(\vec{z}', t)\; J_{q,V}(\vec{y}, \tau)\; J_{q',V}(\vec{0}, \tau)\; \overline{\mathcal{P}}(\vec{z}, 0) \right\} \right\rangle , \tag{4.1}$$

as well as the two-point function

$$C^{\vec{p}}_{2\text{pt}}(t) = a^6 \sum_{\vec{z}',\vec{z}} e^{-i\vec{p}(\vec{z}'-\vec{z})} \left\langle \text{tr}\left\{ P_+ \mathcal{P}(\vec{z}', t)\; \overline{\mathcal{P}}(\vec{z}, 0) \right\} \right\rangle . \tag{4.2}$$

The phase factor $e^{-i\vec{p}(\vec{z}'-\vec{z})}$ selects proton states with the desired three-momentum $\vec{p}$. The operator $J_{q,V}(\vec{y}, \tau)$ is the Euclidean version of the vector current (2.14), and P_+ projects onto positive parity. The interpolating operators $\mathcal{P}(\vec{z}', t)$ $\left(\overline{\mathcal{P}}(\vec{z}, 0)\right)$ annihilate (create) a baryon with the quantum numbers of the proton, i.e. spin $J = 1/2$ and isospin $I = 1/2$:

$$\begin{aligned} \overline{\mathcal{P}}(\vec{x}, t) &= \epsilon_{abc}\; \left[\bar{u}_a(x)\; C\gamma_5\; \bar{d}^T_b(x)\right] \bar{u}_c(x)\big|_{x^4=t} , \\ \mathcal{P}(\vec{x}, t) &= \epsilon_{abc}\; u_a(x) \left[u^T_b(x)\; C\gamma_5\; d_c(x)\right]\big|_{x^4=t} , \end{aligned} \tag{4.3}$$

where C is the charge conjugation matrix in spinor space. The traces in (4.1) and (4.2) are taken with respect to the open spinor indices introduced by the quark fields u_a and $\bar{u}_c$. We denote the time separation between the source and current insertions as τ. The ground state matrix element (2.13) can be extracted by considering large time separations:

$$M_{qq',VV}(p, y)\Big|_{y^0=0} = 2V\sqrt{m^2 + \vec{p}^2}\; \frac{C^{VV,\vec{p}}_{4\text{pt},qq'}(\vec{y}, t, \tau)}{C^{\vec{p}}_{2\text{pt}}(t)}\Bigg|_{0 \ll \tau \ll t} . \tag{4.4}$$

id	β	a[fm]	$L^3 \times T$	κ_l, κ_s	$m_{\pi,K}$[MeV]	$m_\pi La$	configs.
H102	3.4	0.0856	$32^3 \times 96$	0.136865, 0.136549339	355, 441	4.9	2037

Table 1. Details of the CLS ensemble used for the present study. Only 990 configurations were used to generate the four-point functions we are analyzing.

The four-point function (4.1) receives contributions from several Wick contractions of the quark fields, which are shown in Figure 4. Different combinations of these contractions contribute to the matrix elements:

$$\begin{aligned} M_{uu,ij}(p,y)\,\big|_{y^0=0} &= C^{ij,\vec{p}}_{1,uuuu}(\vec{y}) + C^{ij,\vec{p}}_{2,u}(\vec{y}) + C^{ji,\vec{p}}_{2,u}(-\vec{y}) \\ &\quad + S^{ij,\vec{p}}_{1,u}(\vec{y}) + S^{ji,\vec{p}}_{1,u}(-\vec{y}) + S^{ij,\vec{p}}_{2}(\vec{y}) + D^{ij,\vec{p}}(\vec{y})\,, \\ M_{dd,ij}(p,y)\,\big|_{y^0=0} &= C^{ij,\vec{p}}_{2,d}(\vec{y}) + C^{ji,\vec{p}}_{2,d}(-\vec{y}) \\ &\quad + S^{ij,\vec{p}}_{1,d}(\vec{y}) + S^{ji,\vec{p}}_{1,d}(-\vec{y}) + S^{ij,\vec{p}}_{2}(\vec{y}) + D^{ij,\vec{p}}(\vec{y})\,, \\ M_{ud,ij}(p,y)\,\big|_{y^0=0} &= C^{ij,\vec{p}}_{1,uudd}(\vec{y}) + S^{ij,\vec{p}}_{1,u}(\vec{y}) + S^{ji,\vec{p}}_{1,d}(-\vec{y}) + D^{ij,\vec{p}}(\vec{y})\,, \end{aligned} \tag{4.5}$$

where $i = j = V$ in the present context. A detailed derivation and listing of all matrix elements as well as the method of computation of the Wick contractions are given in [6].

The bare lattice operator $J^{\text{latt}}_{q,V}(y)$ is renormalised by the factor Z_V, which includes the conversion to the $\overline{\text{MS}}$-scheme:

$$J^{\overline{\text{MS}}}_{q,V}(y) = Z_V\, J^{\text{latt}}_{q,V}(y)\,. \tag{4.6}$$

Since the vector current has a zero anomalous dimension, Z_V is scale independent.

4.2 Lattice setup

In this study we reuse the data that have been generated in the context of [6]. The simulation includes 990 configurations of the H102 ensemble provided by the CLS Collaboration [22], with a lattice volume of $32^3 \times 96$ and open boundary conditions in time direction, where the Lüscher-Weisz gauge action and $n_f = 2+1$ Sheikoleslami-Wohlert fermions have been employed. Further details are given in Table 1.[2]

The renormalization factor for the vector current has been determined in [25] and can be found in table XXIX therein. For $\beta = 3.4$ it is equal to $Z_V = 0.7115$.

The nucleon source and sink were improved by the application of momentum smearing [26] with 250 smearing iterations. To avoid artifacts stemming from the open boundary conditions in time, the source was chosen at $t_{\text{src}} = 48a$. The sink was placed depending on the momentum as specified in table 2. The operators were inserted on all time slices between source and sink for the C_1 contraction and at $\tau = t/2$ for C_2. Excited states were found to be sufficiently suppressed. The nucleon mass was determined to be $m_N = 1.1296(75)$ GeV.

[2] We take $a = 0.0856$ fm for the lattice size in order to be consistent with our previous study [6]. More recent determinations [23, 24] differ from this value by up to 1%, which is of no practical relevance in the present context.

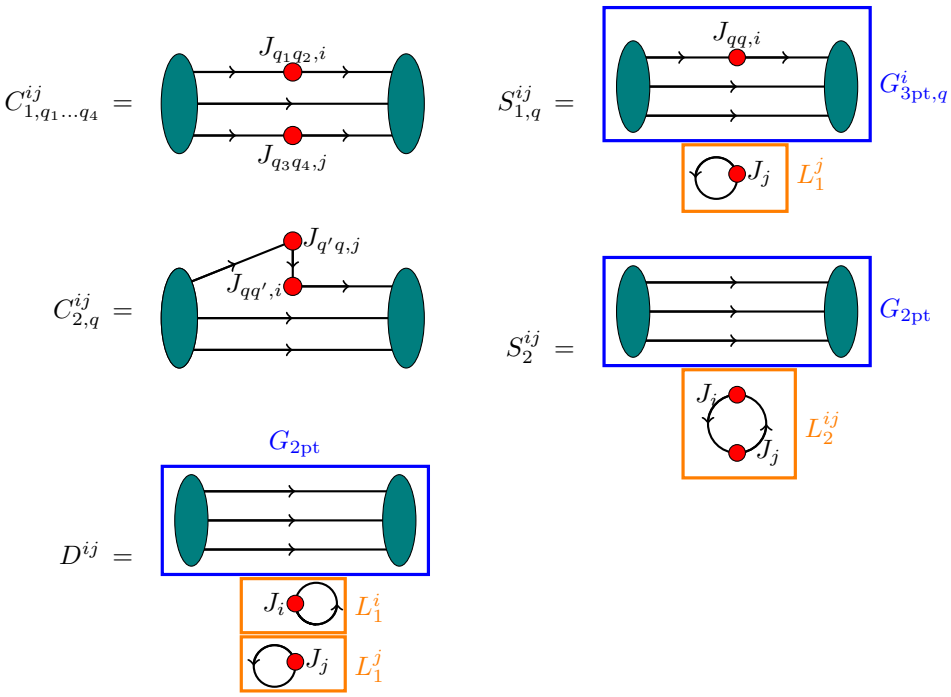

Figure 4. Illustration of the five kinds of Wick contractions (graphs) contributing to a four-point function of a baryon. The explicit contributions for the graphs C_1, C_2 and S_1 depend on the quark flavor of the current insertions (red points). In the case where all quark flavors have the same mass, C_2 only depends on the flavors of the two propagators connected to the source or the sink. These flavors have to be the same for proton-proton matrix elements. For the graphs S_1, S_2 and D we also indicate the parts connected to the proton source and sink, i.e. $G_{3\mathrm{pt}}$ and $G_{2\mathrm{pt}}$ (blue), as well as the disconnected loops L_1 and L_2 (orange). The indices i and j specify the currents and are both equal to V in our context. [Figure taken from Ref. [6]]

Compared to the connected contributions C_1 and C_2, the disconnected terms S_1 and S_2 were found to be small in the considered region of distances $\vec{y}$ (see below) and, thus, are not considered further here. The doubly disconnected contribution D exhibits huge statistical uncertainties, making a determination of this contribution unfeasible at this point in time. Following the argument in [27], we assume that the ratio $D : S_1$ is similar in size to the ratio $S_1 : C_1$, which allows us to neglect the D contribution as well.

In the numerical studies of the present work, we limit ourselves to the matrix element for the flavor combination ud. The other two combinations, uu and dd, include the C_2 graph, which involves a propagator connecting the two current insertions and has considerably larger statistical errors than C_1. This would reduce the stability of the fits we will perform. With the lattice data we have at hand, we therefore refrain from performing fits for the equal-flavor combinations.

With the time separation y^0 between the two currents being zero, the Lorentz invariants

$\vec{P}$	$\lvert\vec{p}\rvert$[GeV]	$(t_{\rm snk} - t_{\rm src})[a]$
$(0,0,0)$	0	12
$(-1,-1,-1)$	0.78	10
$(-2,-2,-2),\ (2,2,-2),\ (2,-2,2),\ (-2,2,2)$	1.57	10

Table 2. Summary of momenta and source-sink separations in our lattice data.

are given by

$$y^2 = -\vec{y}^{\,2}\,, \qquad\qquad \omega = -\vec{p}\,\vec{y}\,, \tag{4.7}$$

so that the Ioffe time is limited to

$$|\omega| \le |\vec{p}\,|\,|\vec{y}\,|\,. \tag{4.8}$$

In order to obtain large ω, one hence needs large proton momenta. For reasons given below, these are chosen in the direction of the lattice diagonals:

$$\vec{p} = \frac{2\pi\vec{P}}{La}\,, \qquad\qquad \vec{P} = (\pm k, \pm k, \pm k)\,, \qquad\qquad k = 0, 1, 2\,, \tag{4.9}$$

where $L = 32$ is the spatial lattice extent and $a = 0.0856\,\text{fm}$ is the lattice spacing. This leads to the physical momenta listed in table 2. As the signal gets worse for larger momenta, the calculation was repeated four times for $k = 2$, using four of the eight possible choices of diagonals. With the momenta (4.9) the bound (4.8) becomes $|\omega| \le 2.72\,|\vec{y}\,|\,/(4a)$.

Let us note that the improved interpolating operators suggested in [28] should allow us in the future to access significantly larger momenta and thus larger ω.

4.3 Data analysis

Having extracted the tensor components of the two-current matrix element from (4.4), we determine the invariant function $A_{q_1q_2}(\omega, y^2)$ by solving the system of linear equations in (2.15). Since this system is overdetermined, we solve it by χ^2 minimization. We can test for lattice artifacts from discretization at small y and from finite-size effects at large y by investigating to which extent the values of $A_{q_1q_2}$ fitted to the continuum relation (2.15) depend only on the invariants y^2 and ω. Specifically, we tested for a dependence on the direction of $\vec{y}$ (anisotropy) and on the size of the proton momentum (frame dependence) when y and ω were kept fixed.[3] We found in [6] that lattice artifacts were smallest for $\vec{y}$ close to the space diagonals of the lattice and hence limit our data extraction to distance vectors for which the angle θ between $\vec{y}$ and the nearest lattice diagonal satisfies

$$\cos\theta > 0.9\,. \tag{4.10}$$

. To maximize the reach in ω, we consequently took proton momenta along the lattice diagonals as specified in (4.9).

[3]For ease of writing, we henceforth write y for the distance $\sqrt{-y^2} = |\vec{y}\,|$ when there is no risk of confusion.

To limit discretization and finite size effects, we will consider data only in the region

$$4a \le y \le 16a\,, \tag{4.11}$$

which in physical units approximately corresponds to $0.34\,\text{fm} < y < 1.37\,\text{fm}$. The upper limit on y corresponds to half the lattice size. Is not too relevant in the sense that for y close to $16a$ statistical uncertainties become rather large, so that this region has little impact on our fits.

5 Modeling the lowest Mellin moment

Our strategy for evaluating Mellin moments $I_{q_1q_2}(\zeta, y^2)$ is to make a model (in the sense of an ansatz) for their functional dependence. For a given model the Fourier transform (2.17) can readily be evaluated. The parameters of the model are then fitted to the data on $A_{q_1a_2}(\omega, y^2)$, which have been extracted from our lattice simulations as described in the preceding section.

To obtain stable fits, we proceed in two steps. We first make an ansatz for the function

$$K_{q_1q_2}(y^2) = A_{q_1q_2}(\omega = 0, y^2) \tag{5.1}$$

and fit its parameters to the data for $\omega = 0$, which has by far the highest statistical precision because it includes the case of zero proton momentum. With this function fixed, we perform fits to the normalized quantity

$$\hat{A}_{q_1q_2}(\omega, y^2) = \frac{A_{q_1q_2}(\omega, y^2)}{A_{q_1q_2}(0, y^2)} \tag{5.2}$$

with the numerator taken from the data and the denominator from the fit of (5.1).

5.1 Factorization of $I(\zeta, y^2)$

We assume that in the y range specified by (4.11) the ζ and y dependence of $I(\zeta, y^2)$ factorizes as

$$I_{q_1q_2}(\zeta, y^2) = J_{q_1q_2}(\zeta)\, K_{q_1q_2}(y^2)\,, \tag{5.3}$$

where $K_{q_1q_2}$ is given in (5.1) and $J_{q_1q_2}$ is an even function of ζ. Fourier transforming (5.3) w.r.t. ζ and comparing with (2.17), we obtain the relation

$$\frac{1}{2\pi} \int_{-1}^{1} \mathrm{d}\zeta\, e^{i\zeta\omega}\, J_{q_1q_2}(\zeta) = \hat{A}_{q_1q_2}(\omega)\,, \tag{5.4}$$

where $\hat{A}_{q_1q_2}$ defined in (5.2) is now y independent. This implies the normalization condition

$$\int_{0}^{1} \mathrm{d}\zeta\, J_{q_1q_2}(\zeta) = \pi\,. \tag{5.5}$$

The different models used for the functional dependence of $J_{q_1q_2}$ are specified below.

We will validate the factorization hypothesis (5.3) by performing fits to (5.4) in narrow bins of y and monitoring to which extent the functions $J_{q_1q_2}$ obtained in this way depend on y. Details are given in Section 6.2.

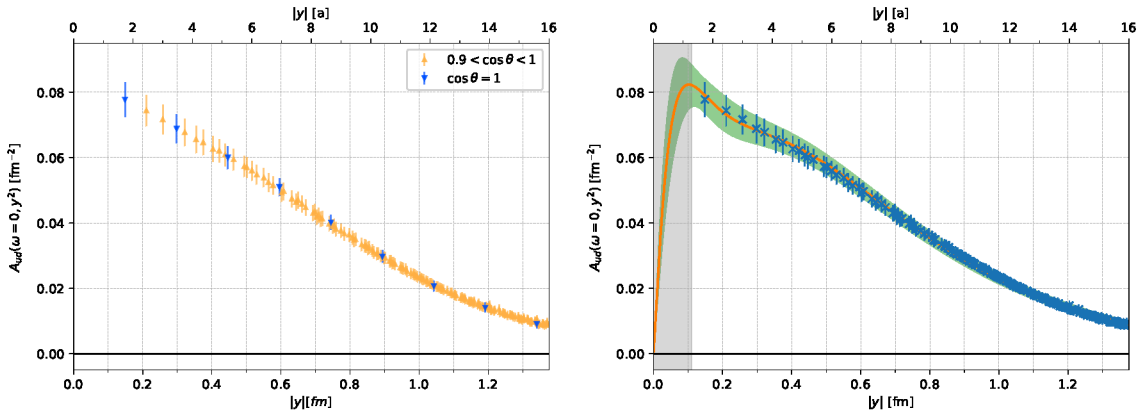

(a) (b)

Figure 5. Lattice data of the invariant function A_{ud} for $\omega = 0$, together with the fit (5.6). The shaded region $y \leq 0.11\,\text{fm}$ is not used in our analysis.

5.2 Dependence on the distance y

From now on we focus on the quark flavor combination $(q_1, q_2) = (ud)$ for the reasons given below Equation (4.5). Our data for $A_{ud}(\omega = 0, y^2) = K_{ud}(y^2)$ is quite precise. Figure 5a shows that there is no systematic difference between data points with $0.9 < \cos\theta < 1$ and data points with $\cos\theta = 1$. This suggests that within the range $0.9 < \cos\theta$ of our data selection, possible anisotropy effects are smaller than statistical errors for this observable.

For the function $K_{ud}(y^2)$ we adapt the fit previously performed in [6], which has the form

$$K_{ud}(y^2) = A_1\,(\eta_1\, y)^\delta\, e^{-\eta_1(y-4a)} + A_2\,(\eta_2\, y)^\delta\, e^{-\eta_2(y-4a)} \qquad \text{for } \sqrt{3}a \leq y \leq 16a \tag{5.6}$$

with $\delta = 1.2$. The fitted parameters A_i and η_i are

$$\begin{aligned} A_1 &= (3.49 \pm 2.37) \times 10^{-4}\,\text{fm}^{-2}\,, & A_2 &= (5.14 \pm 0.04) \times 10^{-2}\,\text{fm}^{-2}\,, \\ \eta_1 &= (17.6 \pm 2.8)\,\text{fm}^{-1}\,, & \eta_2 &= (3.53 \pm 0.03)\,\text{fm}^{-1}\,. \end{aligned} \tag{5.7}$$

In Figure 5b we show the fit together with the data. We emphasize that the y region where the function (5.6) increases with y due to the factor y^δ is never used in our analysis.

At this stage we include data below $y = 4a$ for the following reason. In order to evaluate the number sum rule (2.12), we need values of y down to $0.11\,\text{fm} \approx 1.29a$. Fitting the form (5.6) down to $y = 4a$ would entail a substantial extrapolation error at smaller y. By contrast, a fit down to $y = \sqrt{3}a \approx 1.73a$, which corresponds to the lattice points closest to the origin along the space diagonals, requires only moderate extrapolation.

Together with the factorization assumption (5.3), our fit of K_{ud} relates J_{ud} with the number sum rule as

$$S_{ud}(y_{\text{cut}}) = f(y_{\text{cut}})\, J_{ud}(\zeta = 0) \tag{5.8}$$

with

$$f(y_{\rm cut}) = 2\pi \int_{y_{\rm cut}}^{\infty} \mathrm{d}y\, y\, K_{ud}(y^2) \approx 0.215\,, \tag{5.9}$$

where we take $y_{\rm cut} = 0.11\,\mathrm{fm}$ from (2.11).

The proportionality factor f decreases by about 16% if we integrate over y up to the upper limit $16a$ of our fit, rather than up to ∞. In turn, it decreases by about 11% if we integrate over y from $4a$ to ∞. These numbers may be taken as upper limits (or very conservative estimates) for the uncertainty on f due to (i) extrapolating the fit (5.6) to $y \geq 16a$, and due to (ii) including the region $y \leq 4a$ where discretization effects in our data may be substantial. We also recall from Section 2.2 that the value of $y_{\rm cut}$ in the sum rule integral itself is a matter of choice. Multiplying or dividing $y_{\rm cut}$ by 2 changes the f by less than 5%.

5.3 Dependence on the skewness ζ

The main purpose of this work is to explore different forms for the dependence of Mellin moments on ζ. We now present our models for this dependence.

For ease of notation, we assume that $|\zeta| \leq 1$ throughout this section, bearing in mind that $J_{q_1q_2}(\zeta)$ is zero for $|\zeta| > 1$. The Fourier transform of $J_{q_1q_2}$ is hence to be understood as in (2.17). We will also omit the quark flavor labels henceforth, given that we only perform fits for $(q_1q_2) = (ud)$ as explained above.

The polynomial model is what we used in our previous work [6]. For a given integer N it is given by

$$J_{\rm poly}\,(\zeta) = \pi \sum_{n,m=0}^{N} \zeta^{2n} \left(T^{-1}\right)_{nm} c_m \qquad \text{with } c_0 = 1\,, \tag{5.10}$$

where the $(N+1) \times (N+1)$ matrix T is defined by

$$T_{mn} = 1\big/(1 + 2n + 2m)\,. \tag{5.11}$$

The condition $c_0 = 1$ ensures the normalization condition (5.5), as shown in Section 4.4 of [6]. The model thus has N free parameters, c_1 to c_N. The normalized Fourier transform of (5.10) reads

$$\hat{A}_{\rm poly}\,(\omega) = \sum_{n,m=0}^{N} h_n(\omega)\, \left(T^{-1}\right)_{nm} c_m\,, \tag{5.12}$$

with the functions h_n given by

$$h_n(\omega) = \frac{1}{2} \int_{-1}^{1} \mathrm{d}\zeta\, e^{i\zeta\omega}\, \zeta^{2n} = \sin(\omega)\, s_n(\omega) + \cos(\omega)\, c_n(\omega) \tag{5.13}$$

and

$$s_n(\omega) = \sum_{m=0}^{n} \frac{(-1)^m\,(2n)!}{(2n-2m)!}\, \frac{1}{\omega^{1+2m}}\,, \quad c_n(\omega) = \sum_{m=0}^{n-1} \frac{(-1)^m\,(2n)!}{(2n-2m-1)!}\, \frac{1}{\omega^{2+2m}}\,. \tag{5.14}$$

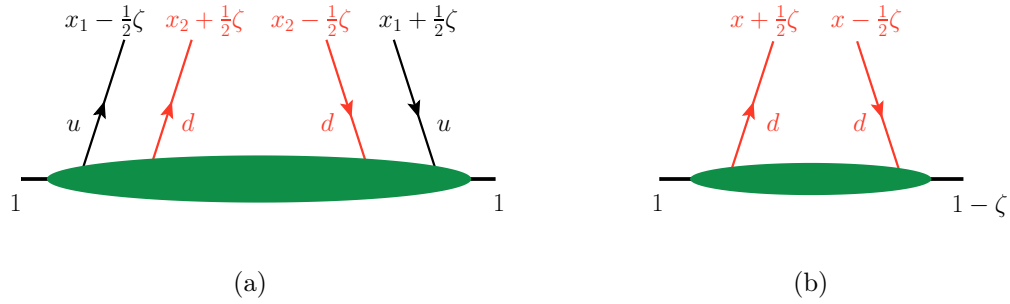

(a) (b)

Figure 6. Comparison between a skewed DPD $F_{ud}\left(x_i, \zeta, y^2\right)$ in the region $x_i \pm \zeta/2 > 0$ (a) and a generalized (a.k.a. skewed) single-parton distribution (b). The notation in [29] uses the variable $X = x + \frac{1}{2}\zeta$ instead of x. All momentum fractions refer to the incoming proton.

We note that the singular behavior of $s_n(\omega)$ and $c_n(\omega)$ for $\omega \to 0$ cancels in the combination (5.13), such that the function $h(\omega)$ is finite at $\omega = 0$, as is obvious from its integral representation.

In [6] we carried out fits with $N = 2$ and $N = 3$ and found their results to be quite close to each other. No clear improvement was observed in the description of the data for $N = 3$, and we regard that version as close to overfitting the data. In the present work we hence restrict ourselves to the case $N = 2$.

The polynomial model does not satisfy the properties we derived in Section 3: the form (5.10) does not vanish for $\zeta \to 1$ (unless one introduces an additional constraint on the polynomial coefficients), nor does it allow for a non-analytic behavior at $\zeta = 0$ or $\zeta = 1$.

When making this ansatz in our previous work, we had in mind the case of generalized single-parton distributions (GPDs).[4] Their Mellin moments *are* in fact polynomials in the skewness parameter ζ, as a consequence of Lorentz invariance [30]. Moreover, they do not generally vanish for $\zeta \to 1$, which already follows from the fact that the lowest moments of quark GPDs are ζ independent. We note that the limit $\zeta \to 1$ is peculiar for GPDs, because for a given invariant momentum transfer t it is always outside the physical region $-t \geq m_p^2 \zeta^2/(1-\zeta)$ in which the proton states are on shell. Despite the apparent similarity between the role of ζ in DPDs and GPDs (see Figure 6), the ζ dependence of these distributions and their Mellin moments is therefore very different.

The following three models are new and have been designed to fulfill the properties discussed in Section 3, i.e. they ensure $I \to 0$ for $\zeta \to 1$, and they allow for a nonanalytic behavior of I at $\zeta = 0$ and $\zeta = 1$.

The power-law model is a rather direct generalization of the polynomial model, given by

$$J_{\text{pow}}(\zeta) = \pi(a+1)\left(1 - |\zeta|\right)^a \qquad \text{with } a > 0\,. \tag{5.15}$$

[4] The following statements hold for both for the skewness parameter ζ of Radyushkin [29] and for the parameter ξ of Ji [30], given their relation $\xi = \zeta/(2-\zeta)$.

Its normalized Fourier transform reads

$$\hat{A}_{\text{pow}}(\omega) = {}_1F_2\left(1; \frac{a+2}{2}, \frac{a+3}{2}; -\frac{\omega^2}{4}\right), \tag{5.16}$$

where ${}_1F_2$ is the hypergeometric function.

The function (5.15) has a spike (i.e. a discontinuous first derivative) at $\zeta = 0$ for all admissible values of a.

The integral model has the form

$$J_{\text{int}}(\zeta) = \pi \frac{\Gamma(a+b+1)}{\Gamma(a+1)\Gamma(b)} \int_{|\zeta|}^1 \mathrm{d}z\, z^{a-1}(1-z)^{b-1} \qquad \text{with } a > 0 \text{ and } b > 0\,, \tag{5.17}$$

and its normalized Fourier transform is given by

$$\hat{A}_{\text{int}}(\omega) = {}_2F_3\left(\frac{a+2}{2}, \frac{a+1}{2}; \frac{3}{2}, \frac{a+b+2}{2}, \frac{a+b+1}{2}; -\frac{\omega^2}{4}\right) \tag{5.18}$$

with the generalized hypergeometric function ${}_2F_3$. The ansatz (5.17) is inspired by the leading-order splitting formula (3.1) for $g \to q\bar{q}$ in conjunction with a PDF behaving as in (3.2), without trying to emulate its detailed features, which are specific to I_{qq} and not directly applicable to I_{ud}.

For $a \leq 1$ the function (5.17) has a spike at $\zeta = 0$, whereas for $a > 1$ it is smooth at that point (with a vanishing first derivative but possible discontinuities of higher odd derivatives).

The cosine model is inspired by the shape of the integral model, but allows for a more direct interpretation of the parameters. It is given by

$$J_{\cos}(\zeta) = \mathcal{N}_{a,b} \cos^b\left(\frac{\pi}{2}|\zeta|^a\right) \text{ with } a > 0 \text{ and } b > 0\,, \tag{5.19}$$

where $\mathcal{N}_{a,b}$ is determined by the normalization condition (5.5). We have not found a closed form for its Fourier transform, which is computed numerically in our fit to the lattice data. Important features of the function $J_{\cos}(\zeta)$ are:

- the parameter a controls the width of the central maximum around $\zeta = 0$,
- the parameter b controls the speed of approaching zero for $|\zeta| \to 1$,
- for $a \leq 1/2$ it has a spike at $\zeta = 0$ and is very sensitive to even small changes in a, whilst for $a > 1/2$ it is smooth at that point,
- for positive half integer a, the function is analytic at $\zeta = 0$.

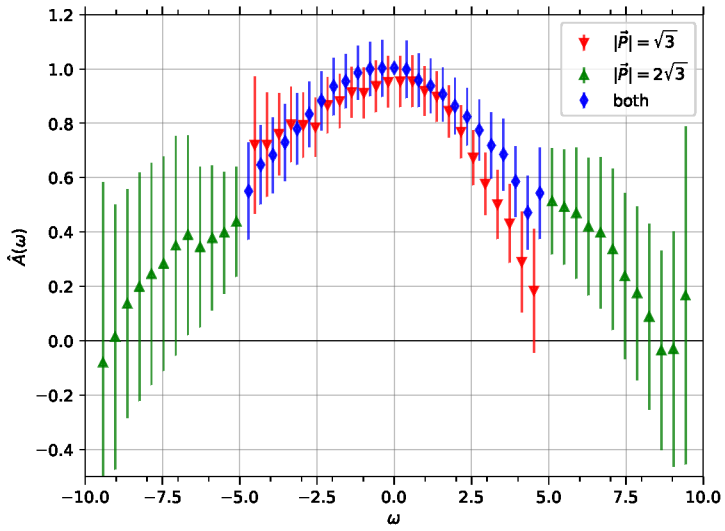

Figure 7. Data for the normalized invariant function $\hat{A}(\omega)$, obtained as described in the text. The different symbols and colors indicate whether a data point receives contributions from proton momenta with $|P| = \sqrt{3}$, $|P| = 2\sqrt{3}$, or from both.

6 Fit results

We now discuss the results of fitting the above models to our lattice data. We performed global fits to the data in the range

$$4a \le y \le 14a\,, \qquad\qquad -2.72\,y/(4a) \le \omega \le 2.72\,y/(4a)\,, \tag{6.1}$$

where the second condition follows from the bound (4.8) and from the range of proton momenta in our simulations. The highest value of $|\omega|$ in the data thus selected is about 9.5. Since statistical errors increase with the proton momentum *and* with the distance y between the currents, the uncertainty on the data is smallest around $\omega = 0$ and grows rather quickly with $|\omega|$. We omit distances $y > 14a$ from the fit because some of the corresponding data points have very large errors.

The fitted data are shown in Figure 7. They are obtained by dividing the data for $A(\omega, y^2)$ in the range (6.1) by the function $K(y^2)$, which is evaluated with the fit specified in (5.6) and (5.7). The errors on the data points are obtained with the jackknife method.

Before turning to our fits, let us discuss some aspects of the data. There are many cases in which several pairs of $\vec{y}$ and $\vec{p}$ have the same ω and y^2, even with our cut (4.10). Some of these pairs are related by symmetries that are exact on the lattice (such as permutations or sign reversal of vector components), but others are not. For the vector $\vec{P} = -(1,1,1)$, which is related to the proton momentum $\vec{p}$ by Eq. (4.9), we obtain for instance the same ω with $\vec{y} = (2,6,7)a$ and $\vec{y} = (3,4,8)a$, both of which have length $y = \sqrt{89}a$.

If we focus on the ω dependence, there are even more configurations that can be combined. For $\vec{P} = -(1,1,1)$, the same ω is for instance obtained with the vectors $\vec{y}$

model	parameters		χ^2/ d.o.f.
polynomial	$c_1 = (9.84 \pm 4.41) \times 10^{-2}$	$c_2 = (6.16 \pm 4.57) \times 10^{-2}$	0.38
power-law	$a = 2.95 \pm 1.10$	—	0.36
integral	$a = 0.37 \pm 2.83$	$b = 2.04 \pm 3.97$	0.35
integral	$a = 0.5$ fixed	$b = 1.23 \pm 1.84$	0.35
integral	$a = 4$ fixed	$b = 7.36 \pm 2.67$	0.40
cosine	$a = 0.29 \pm 1.14$	$b = 1.92 \pm 3.33$	0.35
cosine	$a = 1$ fixed	$b = 5.42 \pm 1.78$	0.38

Table 3. Fit results for our models of the ζ dependence. The low values of χ^2/ d.o.f. are explained in the text. The models are specified in Section 5.3.

just mentioned, with the two vectors $\vec{y} = (3, 6, 6)a$ and $\vec{y} = (4, 4, 7)a$ of length $y = 9a$, with 9 further vectors with different values of y between $9a$ and $10a$, and with yet more vectors with y outside that range. The same ω may also be obtained for different proton momenta; a trivial example is $\vec{P} = -(1, 1, 1)$ with $\vec{y} = (6, 6, 6)a$ and $\vec{P} = -(2, 2, 2)$ with $\vec{y} = (3, 3, 3)a$.

Each data point in Figure 7 results from combining all pairs of $\vec{y}$ and $\vec{p}$ that give the same ω. Even with this combination the result is still statistics limited, especially for larger values of $|\omega|$. Averaging only over pairs of $\vec{y}$ and $\vec{p}$ that are related by lattice symmetries would give points with yet larger statistical errors and not permit us to assess the size of lattice artifacts in the ω dependence.

The figure shows that data points receiving only contributions from $|\vec{P}| = \sqrt{3}$ tend to deviate systematically from those with contributions from $|\vec{P}| = \sqrt{3}$ and $2\sqrt{3}$. We recall that we have only one momentum with $|\vec{P}| = \sqrt{3}$, whereas the data with $|\vec{P}| = 2\sqrt{3}$ includes four momenta and thus benefits from averaging over different spatial directions. We also note that time reversal (which flips the sign of $\vec{p}$ but not of $\vec{y}$) implies that the ω distribution must be symmetric, whilst the central values of the $|\vec{P}| = \sqrt{3}$ data are slightly asymmetric in ω. We shall not investigate this issue further, because the observed deviations are not significant within statistical errors.

In Table 3 we list the results of the fits that will be discussed in the following. We note that the χ^2 of the data was computed *without* taking into account the statistical correlations between data points at different ω. This is because the corresponding correlation matrix is very close to singular, such that its inversion would be affected by severe instabilities. With correlations between data points being neglected, the resulting values of χ^2 per degree of freedom are significantly below 1 in all our fits.

In the left panels of the following figures, we show the fits of $\hat{A}(\omega)$ with their error bands, together with the fitted data points. In the right panels of the same figures, we show the resulting value of $J(\zeta)$, multiplied by the factor f from (5.9). We recall that, according to the number sum rule (2.12), one should have $fJ(\zeta = 0) = 2$ up to corrections of parametric order α_s^2 or $(\Lambda y_{\text{cut}})^2$.

6.1 Comparison of models

The fit results for the polynomial and the power-law model are shown in Figure 8. Both fits give a good description of the data. We note that at large $|\omega|$ they both yield rather narrow error bands compared with the errors on the data points. We observe that the two models behave rather differently in the $|\omega|$ region where we have no data (or data with huge errors), with pronounced oscillations occurring in the polynomial model.[5] In the Fourier conjugate space, these differences are reflected by pronounced differences between the fit results around $\zeta = 0$. Whereas the polynomial model is smooth at that point by construction, the power-law model exhibits a clear spike. At $|\zeta| \to 1$ the polynomial model results in a nonzero value of the Mellin moment, at least within 1σ uncertainties. Based on our arguments in Section 3, we hence disfavor this fitting ansatz on physical grounds.

Figure 9 shows that the two fits agree within their uncertainties for $\hat{A}$ up to $|\omega| \sim 7$. They yield similar results for the Mellin moment at intermediate $|\zeta|$ but differ qualitatively for $|\zeta|$ close to 0 or to 1. Already at this stage we can conclude that in ζ space the uncertainty bands of an individual fit can significantly misrepresent the actual uncertainty on the Mellin moment. At $\zeta = 0$, both fits are consistent with the sum rule value of 2, although for the power-law model this value is at the lower end of the uncertainty band.

It is interesting to note that, broadly speaking, the two fits have error bands of similar size, both in ω and in ζ space, despite the fact that the polynomial model has two and the power-law model one free parameter. This shows that the amount of flexibility of the functional form is crucial for the behavior of the fit, at least with data of the quality we are working with.

The fit results for the integral and cosine models are shown separately in Figure 10 and together in Figure 11. Quite remarkably, both the central values and the error bands agree almost perfectly between the two fits, despite the apparent difference between the functional forms (5.17) and (5.19).

The fits describe the data well. Their error bands become broad at large $|\omega|$, at variance with the polynomial and power-law fits. Correspondingly, we find a *huge* uncertainty on the Mellin moment around $\zeta = 0$ in the right panels of Figure 10. If we accept that these fits adequately represent the uncertainty of our lattice data at large $|\omega|$, we must conclude that the data does not permit a reconstruction of the Mellin moments at the point $\zeta = 0$ without further theory input. Interestingly, the fit uncertainty on the Mellin moment is extremely large only in a narrow range $|\zeta| \lesssim 0.05$, whereas for larger skewness it is of moderate size.

Constrained fits. For the flavor combination ud (but not for equal quark flavors) one may opt to *use* the number sum rule (2.12) as a theory input to the fit. To explore this option, we performed a series of fits to the integral and cosine models with their respective parameters a fixed to a prior value. We find that the fit results for $fJ(\zeta = 0)$ are close to the sum rule value 2 if we impose $a = 4$ in the integral model (5.17) and $a = 1$ in the cosine model (5.19). In Table 3 we see that both constrained fits have a slightly higher χ^2 than their two-parameter counterparts, but still provide a good description of the data. This is

[5] Such oscillations could be anticipated from the functional form in (5.13).

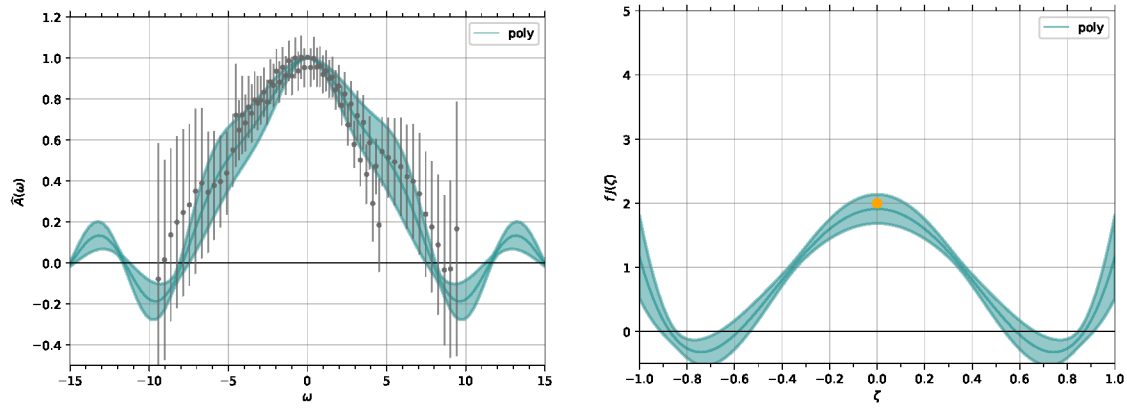

(a) polynomial model

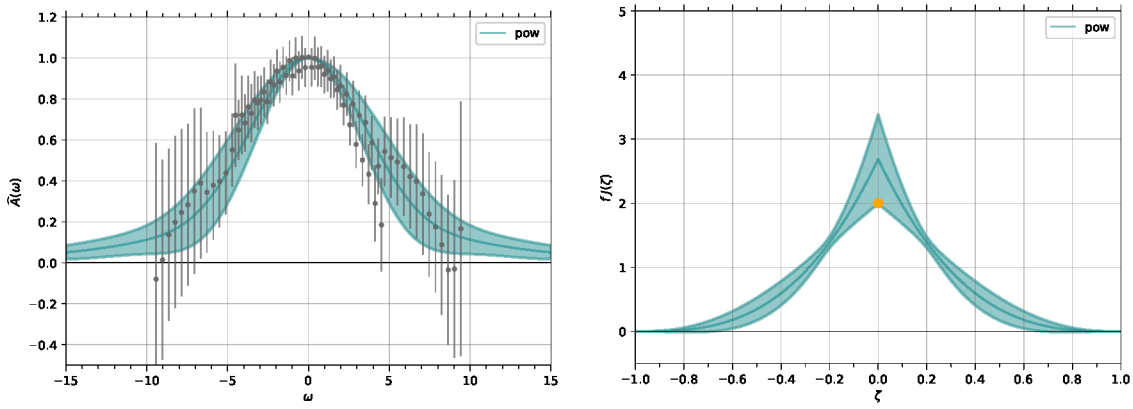

(b) power-law model

Figure 8. Fit results for the polynomial and power-law models. Left panels show the fit and data vs. Ioffe time ω and right panels show the fit results after a Fourier transformation to the skewness ζ. The plots on the right are normalized such that the number sum rule requires the value 2 at $\zeta = 0$, which is indicated by an orange dot. Further explanations are given in the text.

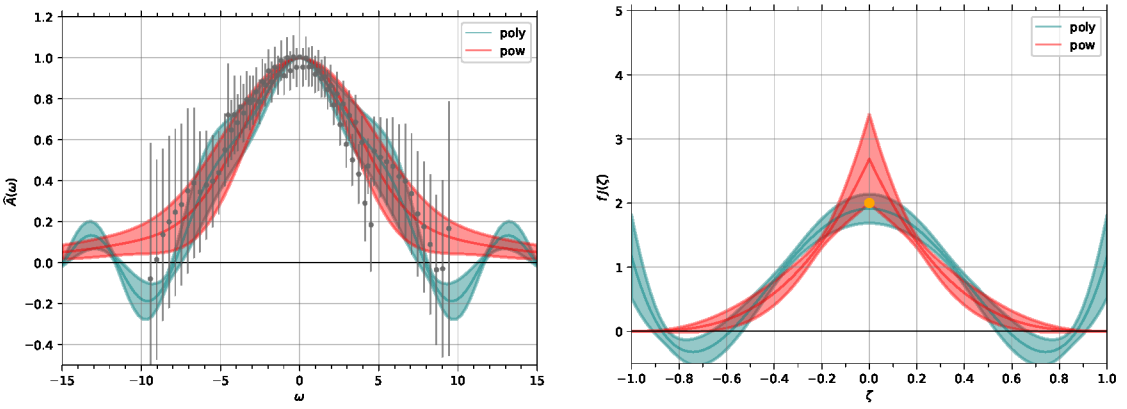

Figure 9. Comparison of the fit results shown in Figure 8. The polynomial model is shown in blue and the power-law model in red.

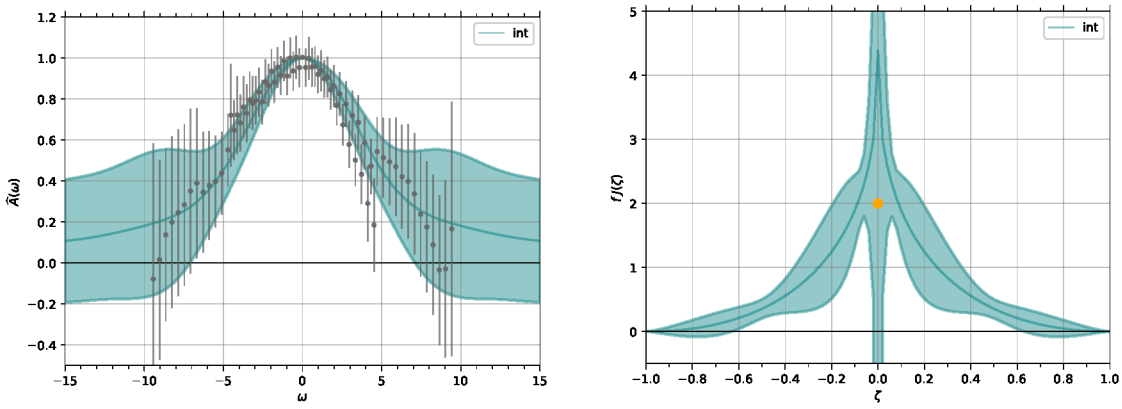

(a) integral model

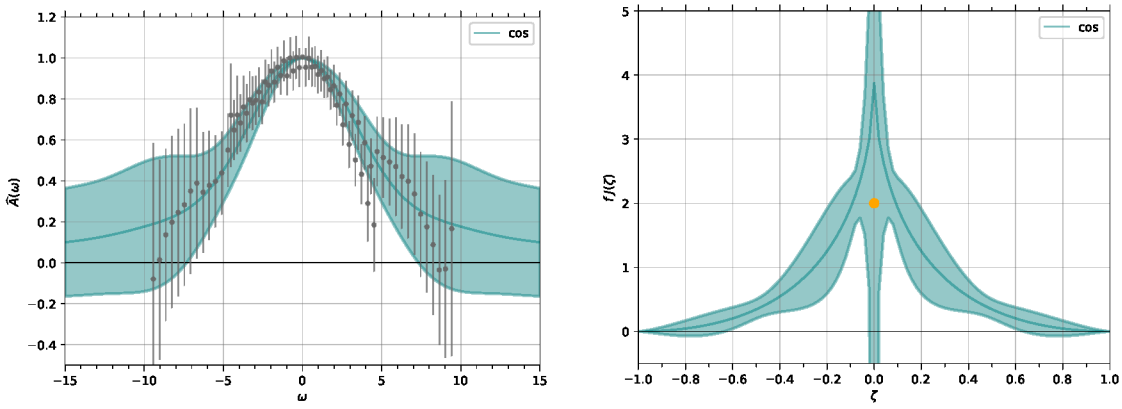

(b) cosine model

Figure 10. As Figure 8, but for the integral and cosine models.

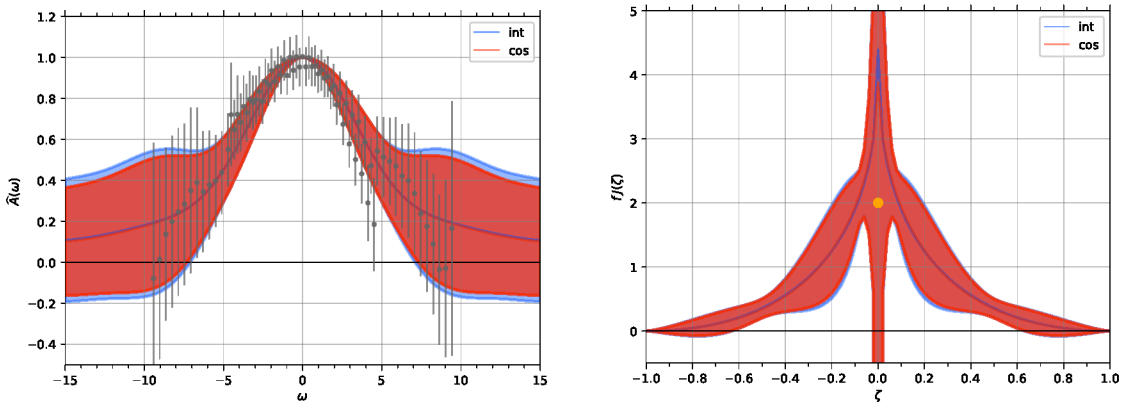

Figure 11. Comparison of the fit results shown in Figure 10. The blue and red curves for the central values are barely distinguishable.

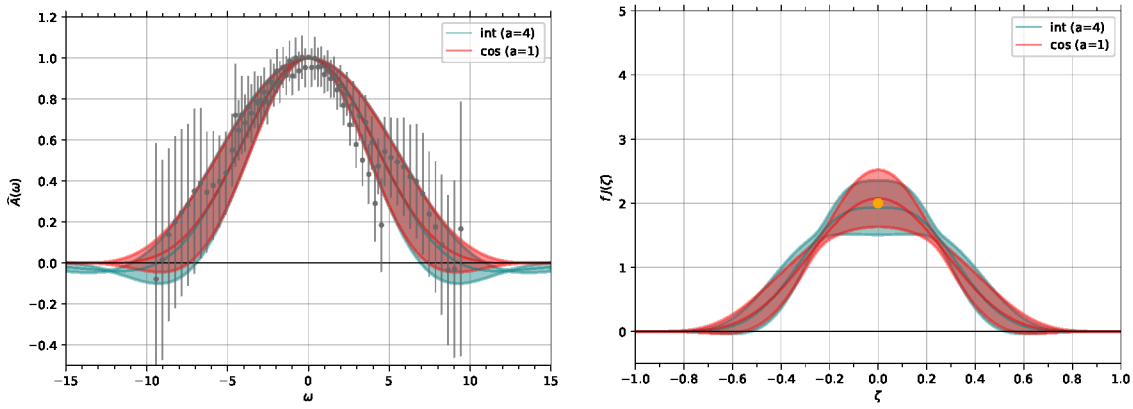

(a) integral and cosine models with fixed a

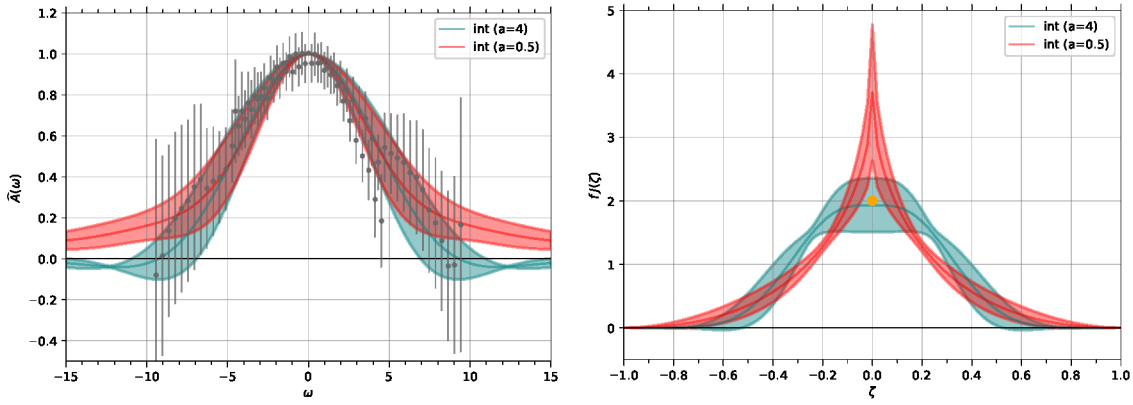

(b) integral model with fixed a

Figure 12. As Figure 10, but for fits with one fixed and one free parameter.

also seen in Figure 12a, which additionally shows that the two constrained fits are quite similar in their central values and error bands. The bands are significantly reduced with respect to the two-parameter fits, as is evident from the comparison with Figure 11.

For the integral model we also performed a constrained fit with fixed $a = 0.5$, which is close to the fitted value of a in the two-parameter fit. The result is compared with the case $a = 4$ in Figure 12b. We see that the two fits differ noticeably at large $|\omega|$ and result in a quite different behavior of the Mellin moment for central values of ζ. The fit with $a = 0.5$ has a spike at $\zeta = 0$ and misses the sum rule value within its 1σ uncertainties.

The results of our fits for the sum rule value $fJ(\zeta = 0)$ are collected in Table 4, where we see again the huge uncertainties on this value obtained with the two-parameter versions of the integral and cosine models.

Also shown in that table are the fit results for another quantity of physical interest,

model	fixed params.	$S_{ud} = fJ_{ud}(\zeta = 0)$	$100\langle\zeta^2\rangle$	χ^2 / d.o.f.
polynomial	—	1.91 ± 0.22	9.67 ± 3.93	0.38
power-law	—	2.67 ± 0.70	6.84 ± 2.58	0.36
integral	—	4.4 ± 938.4	7.30 ± 3.14	0.35
integral	$a = 0.5$	3.69 ± 1.06	7.14 ± 2.67	0.35
integral	$a = 4$	1.92 ± 0.42	6.13 ± 2.36	0.40
cosine	—	3.9 ± 262.2	7.30 ± 3.08	0.35
cosine	$a = 1$	2.07 ± 0.45	6.34 ± 2.49	0.38

Table 4. Results of the fits in Table 3 for the value S_{ud} of the number sum rule and for the average value of ζ^2 defined in (6.2).

namely

$$\langle\zeta^2\rangle = \frac{\int_0^1 \mathrm{d}\zeta\, \zeta^2\, I(\zeta, y^2)}{\int_0^1 \mathrm{d}\zeta\, I(\zeta, y^2)} = -\frac{\partial^2}{\partial\omega^2}\hat{A}(\omega, y^2)\bigg|_{\omega=0}, \tag{6.2}$$

which may be interpreted as the average[6] value of ζ^2. In general $\langle\zeta^2\rangle$ depends on the distance y, but this dependence is absent if we adopt the factorization hypothesis (5.3).

We see in the table that the results for $\langle\zeta^2\rangle$ agree within uncertainties for all our fits, much better than the results for the sum rule value $fJ(\zeta = 0)$. To understand this, we observe in Equation (6.2) that $\langle\zeta^2\rangle$ depends on the behavior of $\hat{A}(\omega, y^2)$ around $\omega = 0$, where our lattice data is quite precise. By contrast, the Mellin moment at $\zeta = 0$ corresponds an integral over all ω and is sensitive to $\hat{A}$ at large ω, where the data becomes increasingly noisy or is missing altogether.

The grand average of $\langle\zeta^2\rangle$ over all fits is around 0.07 (with the largest deviation from the polynomial model) and thus quite small. This is consistent with our argument from Section 3 that $I(\zeta, y^2)$ should decrease rather quickly for $\zeta \to 1$ and makes this statement more quantitative.

6.2 Testing factorization in ζ and y

To test whether the hypothesis (5.3) of a factorized dependence of $I(\zeta, y^2)$ on ζ and y is adequate, we perform "local" fits of the ζ dependence in narrow bins of y. Specifically, we group the lattice data into intervals $(i - 0.5)\, a \le |y| \le (i + 0.5)\, a$ with $i = 4$ to 14 and fit them to the same models for the ζ dependence as before.

The resulting values and errors for $fJ(\zeta = 0)$ and $\langle\zeta^2\rangle$ are shown respectively in Figures 13 and 14 for those fits where the value of $fJ(\zeta = 0)$ has an acceptable uncertainty and is consistent with the number sum rule.

We see that there is no significant indication for a y dependence of either quantity. The errors of the local fits tend to increase when y becomes small, which is due to the decreasing range of ω in that limit. We conclude that our factorized ansatz for the ζ and y dependence

[6] Strictly speaking, the interpretation as an "average" in the statistical sense requires $I(\zeta, y^2) \ge 0$, which is the case for the central values of all our fits, except for the polynomial model.

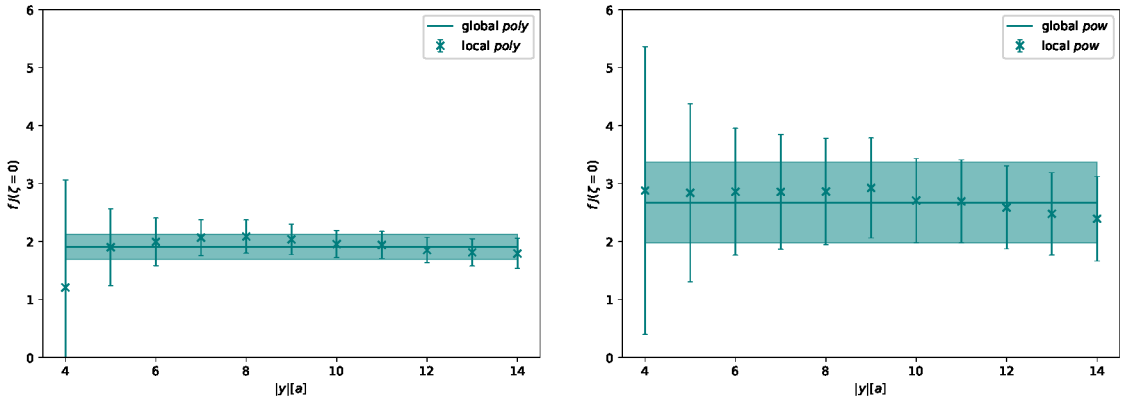

(a) polynomial model

(b) power-law model

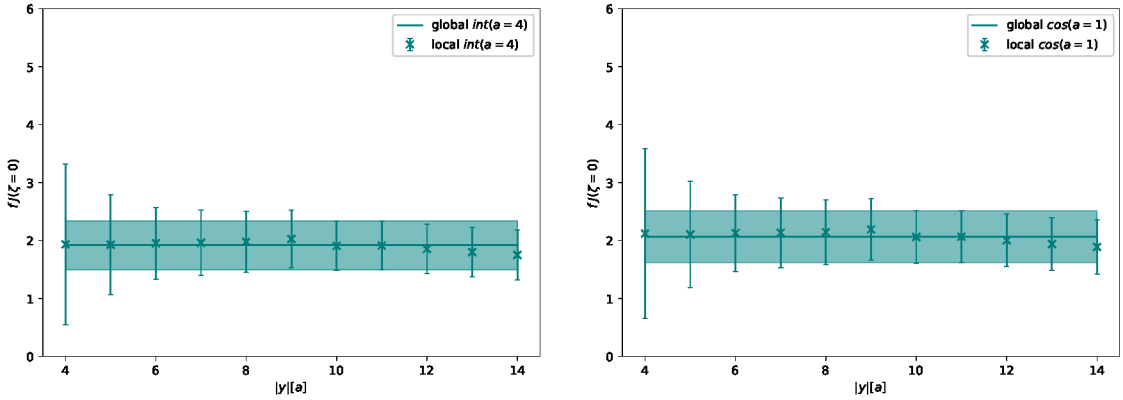

(c) integral model with fixed $a = 4$

(d) cosine model with fixed $a = 1$

Figure 13. Results for $S_{ud} = fJ_{ud}(\zeta = 0)$ from fits restricted to bins in y of width a. The bands indicate the results of the global fits over all y from $4a$ to $14a$.

is good enough for data of the quality we have analyzed. Note that this is equivalent to a factorized form of the ω and y dependence of the invariant function $A(\omega, y^2)$.

7 Summary

Reconstructing Mellin moments of DPDs from lattice data requires the evaluation of an integral of the data over a Ioffe time parameter ω. We can generalize DPDs to asymmetric parton kinematics, such that their Mellin moments are obtained by a Fourier transform of the data from ω to the skewness parameter ζ, with $\zeta = 0$ corresponding to the DPDs relevant for double parton scattering. We have derived two important properties of the dependence on this parameter: the Mellin moments should vanish rather quickly as $|\zeta| \to 1$, and they can be nonanalytic functions of ζ at 0 and ± 1.

In our previous work [6] we had assumed that the Mellin moments are polynomials in ζ, which is at odds with both properties just mentioned. In the present work we have explored

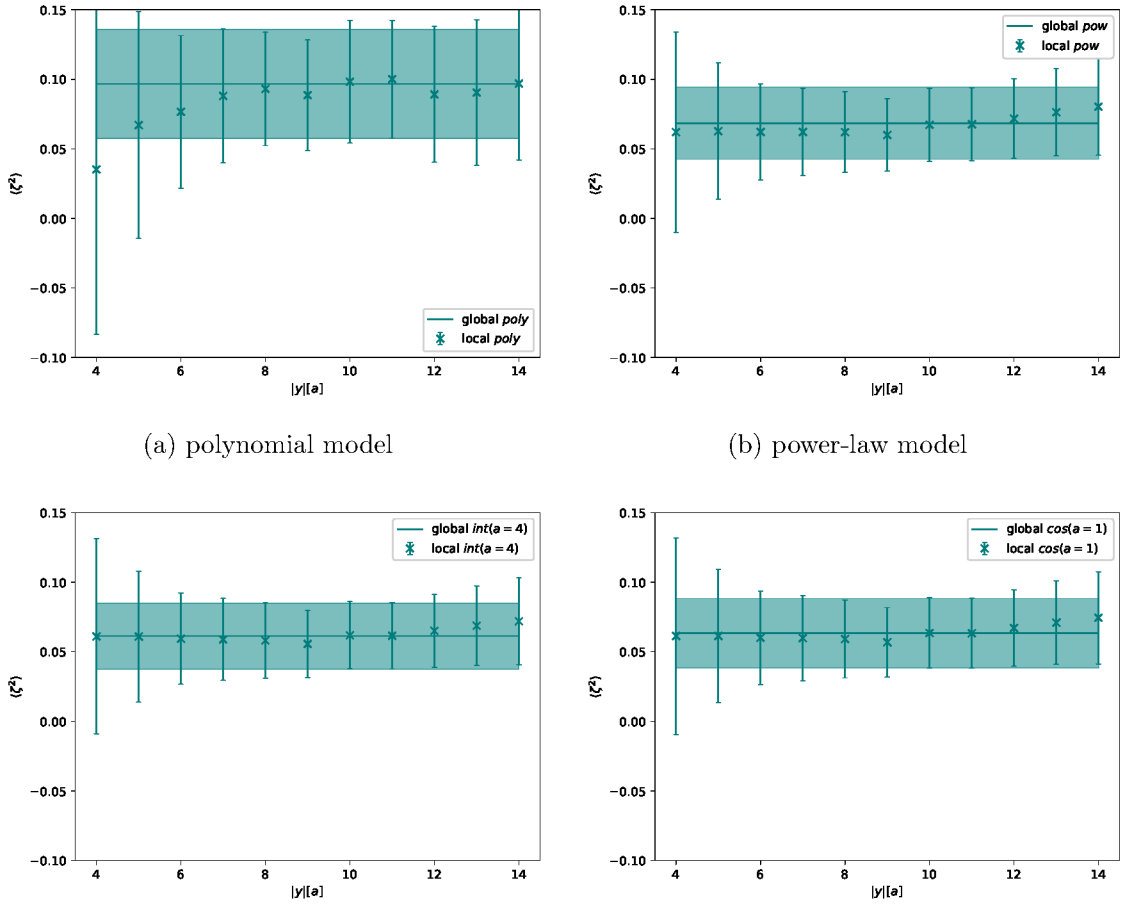

(a) polynomial model

(b) power-law model

(c) integral model with fixed $a = 4$

(d) cosine model with fixed $a = 1$

Figure 14. As Figure 13, but for $\langle \zeta^2 \rangle$.

several model functions for the ζ dependence that are consistent in this respect. We fitted the parameters of these functions to our previously generated lattice data for unpolarized parton pairs in the flavor combination ud, which has the highest statistical precision among all channels analyzed in [6, 7].

We obtain good fits for all considered models. With the flexible forms of our new functions, the fits with two free parameters lead to a huge uncertainty in the reconstructed Mellin moments at $\zeta = 0$, with errors of several hundred units for a value that should be equal to 2 according to the number sum rule for u and d quarks in the proton. Fixing one parameter in these models such that the sum rule is satisfied, we still obtain a good description of the data, with a smooth behavior of the Mellin moments around $\zeta = 0$. The one-parameter model function $\propto (1 - |\zeta|)^a$ admits a good fit to the data, with a Mellin moment that has a spike at $\zeta = 0$ and a value just about consistent with the sum rule. We must conclude that with the lattice data presently at our disposal, we cannot reconstruct Mellin moments at $\zeta = 0$ without additional theory input. To improve on this situation,

one would need data with significantly better precision at high $|\omega|$, i.e. at large proton momenta and large distances y.

Whilst one needs $\zeta = 0$ to make direct contact with double parton scattering, our results for Mellin moments at nonzero ζ still contain relevant information about the joint distribution of two partons inside a proton. As an example, we find that all our fits are consistent with an average value $\langle \zeta^2 \rangle \sim 0.07$ in the Mellin moment $I_{ud}(\zeta, y^2)$, which indicates that parton configurations with small $|\zeta|$ are more likely than those with large $|\zeta|$.

We recall that our studies [6, 7] revealed interesting patterns of small or large correlations between the two partons in their spin and flavor. These correlations were best seen in the precise correlation functions at $\omega = 0$, which according to (2.17) correspond to integrating the associated Mellin moment over all ζ. With the above finding, it is not implausible to assume that features of moments integrated over ζ are not too different from those of the moments at $\zeta = 0$.

In the introduction we mentioned the prospect to obtain more detailed and direct information about DPDs from lattice simulations of the associated quasi-distributions [15, 16] (one may also think of studies using pseudo-distributions). Such distributions depend on three variables that have the nature of Ioffe times, see e.g. Equation (4.1) in [15]. Two linear combinations of those are related by a Fourier transform to the parton momentum fractions x_1 and x_2 in the DPD, whilst a third combination plays a similar role as the parameter ω in the present work. One may therefore expect that the lessons of our study bear some relevance for lattice investigations of DPDs beyond their Mellin moments.

A Skewed DPDs in the short-distance limit

In this appendix we derive the results (3.1) and (3.5) used in Section 3. As in that section, we take $\zeta \geq 0$ without loss of generality. The splitting process $g \to q\bar{q}$ contributes to the distribution $F_{q\bar{q}}$ at leading order in α_s. Evaluation of the graph in Figure 3a gives

$$F_{q\bar{q}}^{\text{sp,LO}}(x_1, x_2, \zeta, y^2) = C\, f_g(x_+)\, \frac{x_+^2 + x_-^2 - \zeta^2}{2x_+^3} \tag{A.1}$$

in the region $x_1 \geq \frac{1}{2}\zeta$, $x_2 \geq \frac{1}{2}\zeta$, $x_1 + x_2 \leq 1$, where we have abbreviated

$$C = \frac{1}{\pi |y^2|}\, \frac{\alpha_s}{2\pi}\, T_F\,, \qquad\qquad x_\pm = x_1 \pm x_2\,. \tag{A.2}$$

A detailed derivation of (A.1) for the case $\zeta = 0$ is given in sections 5.2.2 and 5.3.1 of [4], and it is easy to generalize the corresponding calculation to nonzero ζ.

Integrals of (A.1) over the parton momentum fractions are readily evaluated after changing variables from x_1 and x_2 to x_+ and x_-. The region $x_1 \geq \frac{1}{2}\zeta$, $x_2 \geq \frac{1}{2}\zeta$, $x_1 + x_2 \leq 1$ corresponds to $\zeta \leq x_+ \leq 1$, $-(x_+ - \zeta) \leq x_- \leq x_+ - \zeta$. Carrying out the integral over x_- and renaming x_+ to z, we obtain

$$\int_{\zeta/2}^{1} \mathrm{d}x_1 \int_{\zeta/2}^{1-x_1} \mathrm{d}x_2\, F_{q\bar{q}}^{\text{sp,LO}}(x_1, x_2, \zeta, y^2) = C \int_{\zeta}^{1} \mathrm{d}z\, f_g(z)\, \frac{1}{3}\Big(1 - \frac{\zeta}{z}\Big)^2 \Big(2 + \frac{\zeta}{z}\Big) \tag{A.3}$$

and

$$\int_{\zeta/2}^{1} \mathrm{d}x_1\, x_1 \int_{\zeta/2}^{1-x_1} \mathrm{d}x_2\, x_2\, F_{q\bar{q}}^{\mathrm{sp,LO}}(x_1, x_2, \zeta, y^2)$$
$$= C \int_{\zeta}^{1} \mathrm{d}z\, z^2\, f_g(z)\, \frac{1}{60} \left(1 - \frac{\zeta}{z}\right)^2 \left(6 + \frac{12\zeta}{z} - \frac{2\zeta^2}{z^2} - \frac{\zeta^3}{z^3}\right). \tag{A.4}$$

To evaluate Mellin moments of F_{qq}, we need this function in its full support region in x_1 and x_2. To this end, we use

$$F_{qq}^{\mathrm{sp,LO}}(x_1, x_2, \zeta, y^2) = \begin{cases} -F_{q\bar{q}}^{\mathrm{sp,LO}}(x_1, -x_2, \zeta, y^2) & \text{for } x_1 \geq \frac{1}{2}\zeta,\ x_2 \leq -\frac{1}{2}\zeta,\ x_1 + |x_2| \leq 1, \\ -F_{q\bar{q}}^{\mathrm{sp,LO}}(x_2, -x_1, \zeta, y^2) & \text{for } x_1 \leq -\frac{1}{2}\zeta,\ x_2 \geq \frac{1}{2}\zeta,\ |x_1| + x_2 \leq 1, \\ 0 & \text{otherwise,} \end{cases} \tag{A.5}$$

where the first line follows from the relation between quark and antiquark operators in the definition of unpolarized DPDs, the second line uses the general symmetry relation $F_{qq}(x_1, x_2, \zeta, y^2) = F_{qq}(x_2, x_1, \zeta, y^2)$, and the last line reflects the support properties of the leading-order splitting graphs (see Section 3.1).

We thus find that the lowest Mellin moment of $F_{qq}^{\mathrm{sp,LO}}$ is given by (-2) times the expression in (A.3). Correspondingly, the Mellin moment of $F_{qq}^{\mathrm{sp,LO}}$ with weight factor $x_1 x_2$ is given by $(+2)$ times the expression in (A.4).

Acknowledgments

We acknowledge the CLS effort for generating the $n_f = 2 + 1$ ensembles in [22], one of which was used for this work. The Feynman graphs in this manuscript were produced with JaxoDraw [31, 32].

This work is in part supported by the Deutsche Forschungsgemeinschaft (DFG, German Research Foundation) – grant number 409651613 (Research Unit FOR 2926) and grant number 493441321.

The work of Christian Zimmermann was supported in part by the U.S. Department of Energy, Office of Science, Office of Nuclear Physics, under Contract No. DE-AC02-05CH11231 that is used to operate Lawrence Berkeley National Laboratory. This work was supported by the Alexander von Humboldt Foundation.

References

[1] P. Bartalini and J. R. Gaunt, *Multiple Parton Interactions at the LHC*, *Adv. Ser. Direct. High Energy Phys.* **29** (2019) .

[2] H.-W. Lin et al., *Parton distributions and lattice QCD calculations: a community white paper*, *Prog. Part. Nucl. Phys.* **100** (2018) 107 [arXiv:1711.07916].

[3] M. Constantinou et al., *Parton distributions and lattice-QCD calculations: Toward 3D structure*, *Prog. Part. Nucl. Phys.* **121** (2021) 103908 [arXiv:2006.08636].

[4] M. Diehl, D. Ostermeier and A. Schäfer, *Elements of a theory for multiparton interactions in QCD*, *JHEP* **03** (2012) 089 [arXiv:1111.0910]. [Erratum: JHEP 03, 001 (2016)].

[5] G. S. Bali, L. Castagnini, M. Diehl, J. R. Gaunt, B. Gläßle, A. Schäfer et al., *Double parton distributions in the pion from lattice QCD*, *JHEP* **02** (2021) 067 [arXiv:2006.14826].

[6] G. S. Bali, M. Diehl, B. Gläßle, A. Schäfer and C. Zimmermann, *Double parton distributions in the nucleon from lattice QCD*, *JHEP* **09** (2021) 106 [arXiv:2106.03451].

[7] D. Reitinger, C. Zimmermann, M. Diehl and A. Schäfer, *Double parton distributions with flavor interference from lattice QCD*, *JHEP* **04** (2024) 087 [arXiv:2401.14855].

[8] X. Ji, *Parton Physics on a Euclidean Lattice*, *Phys. Rev. Lett.* **110** (2013) 262002 [arXiv:1305.1539].

[9] X. Ji, *Parton Physics from Large-Momentum Effective Field Theory*, *Sci. China Phys. Mech. Astron.* **57** (2014) 1407 [arXiv:1404.6680].

[10] A. Radyushkin, *Nonperturbative Evolution of Parton Quasi-Distributions*, *Phys. Lett. B* **767** (2017) 314 [arXiv:1612.05170].

[11] A. V. Radyushkin, *Quasi-parton distribution functions, momentum distributions, and pseudo-parton distribution functions*, *Phys. Rev. D* **96** (2017) 034025 [arXiv:1705.01488].

[12] J.-W. Chen et al., *Large-momentum effective theory's asymptotic extrapolation vs the inverse problem*, *Phys. Rev. D* **113** (2026) 014509 [arXiv:2505.14619].

[13] A.-S. Xiong, J. Hua, Y.-F. Ling, T. Wei, F.-S. Yu, Q.-A. Zhang et al., *Ill-posedness in limited discrete Fourier inversion and regularization for quasi distributions in LaMET*, *Eur. Phys. J. C* **85** (2025) 1409 [arXiv:2506.16689].

[14] H. Dutrieux, J. Karpie, C. J. Monahan, K. Orginos, A. Radyushkin, D. Richards et al., *Inverse problem in the large momentum effective theory framework*, *Phys. Rev. D* **113** (2026) 074524 [arXiv:2504.17706].

[15] M. Jaarsma, R. Rahn and W. J. Waalewijn, *Towards double parton distributions from first principles using Large Momentum Effective Theory*, *JHEP* **12** (2023) 014 [arXiv:2305.09716].

[16] J.-H. Zhang, *Double Parton Distributions from Euclidean Lattice*, arXiv:2304.12481.

[17] R. L. Jaffe, *Parton Distribution Functions for Twist Four*, *Nucl. Phys. B* **229** (1983) 205.

[18] J. R. Gaunt and W. J. Stirling, *Double Parton Distributions Incorporating Perturbative QCD Evolution and Momentum and Quark Number Sum Rules*, *JHEP* **03** (2010) 005 [arXiv:0910.4347].

[19] J. Gaunt, *Double parton scattering in proton-proton collisions*, Ph.D. thesis, Cambridge U., 2012. 10.17863/CAM.16589.

[20] M. Diehl, P. Plößl and A. Schäfer, *Proof of sum rules for double parton distributions in QCD*, *Eur. Phys. J. C* **79** (2019) 253 [arXiv:1811.00289].

[21] M. Diehl, J. R. Gaunt and K. Schönwald, *Double hard scattering without double counting*, *JHEP* **06** (2017) 083 [arXiv:1702.06486].

[22] M. Bruno et al., *Simulation of QCD with $N_f = 2 + 1$ flavors of non-perturbatively improved Wilson fermions*, *JHEP* **02** (2015) 043 [arXiv:1411.3982].

[23] RQCD collaboration, G. S. Bali, S. Collins, P. Georg, D. Jenkins, P. Korcyl, A. Schäfer et al., *Scale setting and the light baryon spectrum in $N_f = 2 + 1$ QCD with Wilson fermions*, *JHEP* **05** (2023) 035 [arXiv:2211.03744].

[24] A. Conigli, D. Djukanovic, G. von Hippel, S. Kuberski, H. B. Meyer, K. Miura et al., *Precision lattice calculation of the hadronic contribution to the running of the electroweak gauge couplings*, arXiv:2511.01623.

[25] RQCD collaboration, G. S. Bali, S. Bürger, S. Collins, M. Göckeler, M. Gruber, S. Piemonte et al., *Nonperturbative Renormalization in Lattice QCD with three Flavors of Clover Fermions: Using Periodic and Open Boundary Conditions*, *Phys. Rev. D* **103** (2021) 094511 [arXiv:2012.06284]. [Erratum: Phys.Rev.D 107, 039901 (2023)].

[26] G. S. Bali, B. Lang, B. U. Musch and A. Schäfer, *Novel quark smearing for hadrons with high momenta in lattice QCD*, *Phys. Rev. D* **93** (2016) 094515 [arXiv:1602.05525].

[27] G. S. Bali, P. C. Bruns, L. Castagnini, M. Diehl, J. R. Gaunt, B. Gläßle et al., *Two-current correlations in the pion on the lattice*, *JHEP* **12** (2018) 061 [arXiv:1807.03073].

[28] R. Zhang, A. V. Grebe, D. C. Hackett, M. L. Wagman and Y. Zhao, *Kinematically enhanced interpolating operators for boosted hadrons*, *Phys. Rev. D* **112** (2025) L051502 [arXiv:2501.00729].

[29] A. V. Radyushkin, *Nonforward parton distributions*, *Phys. Rev. D* **56** (1997) 5524 [arXiv:hep-ph/9704207].

[30] X.-D. Ji, *Off forward parton distributions*, *J. Phys. G* **24** (1998) 1181 [arXiv:hep-ph/9807358].

[31] D. Binosi and L. Theußl, *JaxoDraw: A Graphical user interface for drawing Feynman diagrams*, *Comput. Phys. Commun.* **161** (2004) 76 [arXiv:hep-ph/0309015].

[32] D. Binosi, J. Collins, C. Kaufhold and L. Theußl, *JaxoDraw: A Graphical user interface for drawing Feynman diagrams. Version 2.0 release notes*, *Comput. Phys. Commun.* **180** (2009) 1709 [arXiv:0811.4113].